Concurrent modes of climate variability linked to spatially compounding wind and precipitation extremes in the Northern Hemisphere

Bastien François[1,*], Khalil Teber[2,*], Lou Brett[3], Richard Leeding[4], Luis Gimeno-Sotelo[5, 6, 7], Daniela I. V. Domeisen[8, 9], Laura Suarez-Gutierrez[9, 10], and Emanuele Bevacqua[11]

[1]Royal Netherlands Meteorological Institute (KNMI), Research and Development Weather and Climate (RDWK), De Bilt, The Netherlands
[2]RSC4Earth, IEF, Leipzig University
[3]Department of Civil and Environmental Engineering, University of Strathclyde, Glasgow, UK
[4]Department of Earth Sciences, Uppsala University, Uppsala, Sweden
[5]Departamento de Estatística e Investigação Operacional, Faculdade de Ciências, Universidade de Lisboa, Lisboa, Portugal
[6]CEAUL - Centro de Estatística e Aplicações, Faculdade de Ciências, Universidade de Lisboa, Lisboa, Portugal
[7]Centro de Investigación Mariña, Environmental Physics Laboratory, Universidade de Vigo, Ourense, Spain
[8]Université de Lausanne, Lausanne, Switzerland
[9]Institute for Atmospheric and Climate Science, ETH Zurich, Zurich, Switzerland
[10]Institut Pierre-Simon Laplace, CNRS, Paris, 75252, France
[11]Department of Compound Environmental Risks, Helmholtz Centre for Environmental Research – UFZ, Leipzig, Germany
[*]These authors contributed equally to this work.

Correspondence: Bastien François (bastien.francois@knmi.nl) and Emanuele Bevacqua (emanuele.bevacqua@ufz.de)

Abstract. Compound wind and precipitation (CWP) extremes often cause severe impacts on human society and ecosystems, such as damage to crops and infrastructure. Spatially compounding events with multiple regions affected by CWP extremes in the same winter can impact the global economy and reinsurance industry, however our understanding of these events is limited. While climate variability modes such as El Niño Southern Oscillation (ENSO) can influence the frequency of precipitation and wind extremes, their individual and combined effects on spatial co-occurrences of CWP extremes across the Northern Hemisphere have not been systematically examined. Here, by combining reanalysis data and climate model simulations, we investigate how two oceanic and two atmospheric variability modes – ENSO, the Atlantic Multidecadal Variability (AMV), the North Atlantic Oscillation (NAO) and the Pacific North American (PNA) – amplify the wintertime (December–February) frequency of daily CWP extremes and associated spatial co-occurrences across the Northern Hemisphere. We find many hotspot regions where concurrent variability mode anomalies significantly amplify wintertime CWP extreme event frequencies compared to single variability modes. By examining the relationships between frequencies of wintertime CWP extremes across regions, we identify dependencies enabling extreme spatially compounding events, that is winters with many regions experiencing CWP extremes. While ENSO is the most influential variability mode for such extreme spatially compounding events, the occurrence of these events increases further when multiple modes of variability are in anomalous phases. In particular, combinations of modes increase both the number of regions and the population exposed to daily CWP extremes in the same winter. For example, combined ENSO- and NAO+ nearly doubles the number of affected regions compared to neutral con-

1

ditions on average. Our analysis highlights the importance of considering the interplay between variability modes to improve risk management and adapt to the impacts of spatially compounding CWP extremes.

1 Introduction

Weather and climate extremes pose severe risks to human health, infrastructure, natural resources, and ecosystem health (IPCC, 2021). Compound weather and climate events, defined as the combination of multiple drivers and/or hazards that contribute to societal or environmental risk, often cause more severe impacts than the respective single hazards (Zscheischler et al., 2018). The Intergovernmental Panel on Climate Change (IPCC) Special Report on Managing the Risks of Extreme Events and Disasters to Advance Climate Change Adaptation (SREX) highlighted the importance of studying compound events to improve modeling and risk estimation of weather impacts (IPCC, 2012). Without considering compound extreme weather events, damages from extreme weather events may be either under- or over-estimated (e.g., van den Hurk et al., 2023; Hillier et al., 2020). A highly studied example of an impactful compound event is hot-dry conditions (e.g., Bevacqua et al., 2022), which are enhanced by land-atmopshere feedback (e.g., Zscheischler and Seneviratne, 2017; Rasmijn et al., 2018; Ridder et al., 2022). Another example is compound wind and precipitation (CWP) extremes that can cause more damage than high winds or precipitation in isolation (e.g., Li et al., 2024). For example, the combination of high winds and rainwater can result in severe damage due to the inflow of water through joints or cracks in building structures (e.g., Blocken and Carmeliet, 2004; Mirrahimi et al., 2015; Martius et al., 2016; Jeong et al., 2020). CWP extremes can lead to a range of other exacerbated impacts, such as increased soil erosion (e.g., Foulds and Warburton, 2007), agricultural and forestry losses (e.g., Van Stan et al., 2011; Ridder et al., 2022), and damage to energy infrastructure and buildings (e.g., Mirrahimi et al., 2015; Jeong et al., 2020). They can also result in economic impacts through insurance and disaster recovery (e.g., van den Hurk et al., 2023; Ciullo et al., 2023), and human fatalities (e.g., Pilorz et al., 2023). Going forward, these CWP extremes are likely to change in frequency and/or intensity due to human-induced climate change (IPCC, 2021).

Alongside co-occurring extremes in the same location, which correspond to *multivariate events* (Zscheischler et al., 2020), another type of compound event involves the simultaneous occurrence of extremes across multiple regions or locations, referred to as *spatially compounding* extremes (Zscheischler et al., 2020). Spatially compounding events are gaining prominence due to the potential to cause widespread impacts on the global food system, disaster management resources, and (re)insurance industries by simultaneously affecting large population and asset (e.g., Singh et al., 2021; Ciullo et al., 2023; Gampe et al., 2024; Bevacqua et al., 2024). For example, widespread spatially compounding flooding throughout nine European countries in June 2013 placed high pressures on trans-national risk reduction and risk transfer mechanisms and €12 billion in losses (Jongman et al., 2014). In cases where simultaneous extreme hazards across multiple regions occur worldwide, global catastrophe risk pooling could help with reducing the severity of economic shocks (Ciullo et al., 2023). While the characteristics of spatially compounding events such as droughts (e.g., Kim et al., 2019; Singh et al., 2021) or floods (e.g., Jongman et al., 2014) have already been studied, our understanding of spatially compounding CWP extremes and their drivers is limited.

To advance our understanding of CWP extremes and their drivers, this study focuses on the Northern Hemisphere due to the high population density and the severe impacts of CWP extremes in this part of the world (e.g., Liberato, 2014; Wahl et al., 2015; Raveh-Rubin and Wernli, 2015). Such compound extremes are most frequent in coastal regions of the Pacific and Atlantic oceans (e.g., Maraun, 2016) and tend to be more frequent and intense in the winter season (e.g., Greeves et al., 2007; Hansen et al., 2019). Consequently, this study focuses on seasonal frequency of daily CWP extremes during December-February. While multiple drivers can lead to CWP extremes, their influence varies across different geographical regions (e.g., Dowdy and Catto, 2017; Zscheischler and Lehner, 2021; Li et al., 2022; Manning et al., 2024). Typical drivers of CWP extremes include atmospheric rivers (e.g., Ralph et al., 2006; Waliser and Guan, 2017), low-pressure systems (e.g., Rappaport, 2000; Seneviratne et al., 2012; Wahl et al., 2015) including tropical (e.g., Cerveny and Newman, 2000; Zhang et al., 2021) and extratropical cyclones (e.g., Raible, 2007; Owen et al., 2021) and fronts (e.g., Raveh-Rubin and Catto, 2019). Accordingly, regions prone to cyclones are particularly exposed to CWP extremes (e.g., Martius et al., 2016; Messmer and Simmonds, 2021; Owen et al., 2021). As an example of the potential costs, the extratropical cyclones Anatol, Lothar and Martin that hit Europe in December 1999 caused damages totaling 13.5 billion USD (adjusted to the value in 2012) and over 150 fatalities (Roberts et al., 2014).

At the global scale, such drivers are modulated by modes of atmospheric and oceanic variability, which represent variations in atmospheric patterns due to internal climate variability. For example, the North Atlantic Oscillation (NAO) and Pacific North American (PNA) are the leading modes of variability affecting wintertime weather in Europe (e.g., Hurrell, 1995) and North America (e.g., Wallace and Gutzler, 1981). During extreme phases of the PNA and NAO, the intensity and location of storms and moisture transport deviate from mean conditions over the Pacific-North American region (e.g., Wallace and Gutzler, 1981; Xie et al., 2020) and the Euro-Atlantic region (e.g., Hurrell et al., 2003; Lodise et al., 2022), respectively. While positive NAO phases intensify westerly winds and shift the North Atlantic storm track toward the northeast, leading to increased storm frequency and intensity over Northern Europe, negative NAO phases weaken the westerlies and amplify storm activity in the Mediterranean region (e.g., Hurrell and Deser, 2010; Priestley et al., 2023). Oceanic modes of variability such as the El Niño Southern Oscillation (ENSO) and the Atlantic Multidecadal Variability (AMV) can further modulate atmospheric modes of variability and CWP extremes. For example, ENSO can influence both the PNA and NAO (e.g., Müller and Roeckner, 2006; Jiménez-Esteve and Domeisen, 2019, 2020) as well as weather systems in many regions worldwide (e.g., van Oldenborgh et al., 2005; Zhao, 2015; Domeisen et al., 2019). The AMV, an alternation of warm and cold sea surface temperatures in the North Atlantic on decadal timescales, has been shown to influence weather in both North America and Europe (e.g., Knight et al., 2006), as well as the long-term variability of the NAO (e.g., Davini et al., 2015). There are complex teleconnections linking the ENSO, NAO, PNA and AMV modes and their influence on weather patterns across the Northern Hemisphere (e.g., Müller and Roeckner, 2006; Toniazzo and Scaife, 2006; Pinto et al., 2009; Davini et al., 2015; Trascasa-Castro et al., 2021; Hu et al., 2023; King et al., 2023; O'Reilly et al., 2024). Some of the modes are specific phenomena that are internally driven, such as ENSO, while others are a representation of the dominant weather and climate variability in a particular region, such as the NAO or the PNA.

Understanding the drivers of CWP extremes is crucial for optimising resource distribution during response efforts, yet research in this area remains limited. Several studies have explored the influence of single or combined mode of variability anomalies on precipitation and wind extremes in isolation, both at regional (e.g., Elsner et al., 2001; Abeysirigunawardena et al., 2009; Kossin et al., 2010; Grimm, 2011) and global scales (e.g., Khouakhi et al., 2016; Gao et al., 2022; Liu et al., 2024). Regarding CWP extremes, some studies have explored the influence of individual variability modes at the regional scale only (e.g., Hillier et al., 2020; Bloomfield et al., 2024), thus not allowing the assessment of the relation between concurrent climate variability modes and spatial co-occurrences of CWP extremes across several regions. In this study, we use reanalyses data and large ensemble climate model simulations from the CESM General Circulation Model (Kay et al., 2015), to investigate the effects of ENSO, NAO, PNA and AMV modes of variability, and their combinations, on the increase in the frequency of December–January–February daily CWP extremes across the Northern Hemisphere. We consider these four modes of variability due to their already-known influence on storm activity and moisture transport in the Northern Hemisphere. As ENSO operates primarily on seasonal timescales (e.g., Schmidt et al., 2001; Camberlin et al., 2001), seasonal mean indices are considered. Specifically, we (1) analyse how different modes of variability increase wintertime regional frequencies (i.e., seasonal counts) of daily CWP extremes across individual regions of the Northern Hemisphere. We then investigate spatially compounding events with many regions under high CWP extreme frequencies in the same winter by examining the effect of (2) dependencies between CWP extremes across different regions and (3) combinations of modes of variability on such spatially compounding events. Finally, we (4) inspect the atmospheric circulation anomalies associated with these compound events. To the best of the authors' knowledge, the present study is the first to investigate CWP extremes and associated spatially compounding events across the Northern Hemisphere as mediated by multiple large-scale modes of variability. We address this research gap by using large ensemble climate model simulations to provide a robust model-based analysis of the effects of rare concurrent variability mode anomalies on low probability daily CWP extremes (e.g., van der Wiel et al., 2019; Singh et al., 2021; Raymond et al., 2022; Bevacqua et al., 2023; Qian et al., 2023; Wang et al., 2023).

The study is structured as follows: Sect. 2 describes the data used, as well as the methodology to analyse the effects of variability modes on CWP extremes and spatially compounding events. Results are provided in Sect. 3. Conclusions, discussions, and perspectives for future research are presented in Sect. 4.

2 Data and Methods

We examine the influence of four variability modes on CWP extremes across 25 selected regions in the Northern Hemisphere defined in the SREX (Iturbide et al., 2020, see Fig. 1). We chose these regions as they are standard reference in IPCC reports, as they encompass areas with relatively homogeneous climatic characteristics (Iturbide et al., 2020). While using these regions does not enable an explicit analysis of dependencies between local-scale CWP extremes and modes of variability, it allows for complementing IPCC assessments.

2.1 Model and reanalysis data

We employ model simulations from the coupled Community Earth System Model (CESM; spatial resolution of $1.25°$ by $1.25°$), which provides forty ensemble members (Kay et al., 2015). These ensemble members are derived from the CESM model under the same model physics and external forcings, with each of the members starting in 1920 and initialised from slightly different initial states, leading to different evolutions from internal climate variability (Maher et al., 2021). Considering multiple members provides a large sample size that allows for assessing the effect of internal climate variability and infrequent combinations of modes of variability on rare compound events (e.g., Bevacqua et al., 2023; Singh et al., 2021). Daily total precipitation and daily mean of wind speed are extracted for the historical period (1950–2005). Simulated data are then extended until 2019 using the emission scenario associated with a radiative forcing of $+8.5\text{W.m}^{-2}$ (RCP 8.5 scenario), resulting in a total of $70 \times 40 = 2800$ years of data. We choose daily averages rather than maxima for wind due to data availability for the CESM simulations.

To evaluate the CESM model, we employ ERA5 reanalysis data (Hersbach et al., 2020) (spatial resolution of $0.25°$) for the period 1959-2019, from which we also extract daily means of wind speed and daily total precipitation for consistency.

Seasonal indices for the two oceanic (ENSO and AMV) and two atmospheric (NAO and PNA) variability modes for both CESM and ERA5 data are calculated from monthly data using the National Center for Atmospheric Research (NCAR) data package Climate Variability Diagnostics Package (CVDP, Phillips et al., 2014). The seasonal indices for the NAO, PNA and AMV are calculated as the mean of the monthly values for December, January and February. For these indices, December is taken from the year $n-1$, while January and February are taken from year n, and the resulting seasonal index is assigned to year n. For ENSO we proceeded similarly, but used November–January averages to account for lagged effects (e.g., Kawamura et al., 2004; Li et al., 2011; Hong Lee et al., 2023). For each mode, we defined their positive and negative phases when the index is above or below its mean by $+1$ standard deviation, respectively, otherwise the phase is considered neutral.

2.2 Methods

2.2.1 CWP extremes

Many techniques have been utilized to characterize CWP extremes, with the selection of a specific method being guided by the research question. For example, the correlation between wind and precipitation has been quantified at daily to seasonal timescales (e.g., Matthews et al., 2014; Luca et al., 2017; Hillier et al., 2020; Bloomfield et al., 2023). Logistic regression models have been applied to quantify the likelihood of a precipitation extreme occurring given the presence of a wind extreme (e.g., Martius et al., 2016). Alternative approaches include examining tail dependence (e.g., Vignotto et al., 2021) and employing impact-focused metrics (e.g., Hillier et al., 2015, 2020; Bevacqua et al., 2021a). The most straightforward approaches include counting extreme wind and precipitation co-occurrences above a given percentile (e.g., Martius et al., 2016; Bevacqua et al., 2021a), or using extremal dependency measures estimating the probability of one variable being extreme given that the other one is extreme (e.g., Coles et al., 1999; Hillier et al., 2015; Owen et al., 2021).

Here, to investigate winter season (December–February) CWP extremes at the grid cell level we derived seasonal counts of daily CWP extremes, defined as wind and precipitation values simultaneously exceeding high thresholds. This results in one count per season per grid cell, which allows for investigating the effect of seasonally-averaged climate variability modes on the counts. We use the 98th percentile of wind and precipitation over the 1950–2019 period for the main analysis based on data from the CESM model. Percentile-based thresholds are frequently used to investigate climate extremes (e.g., Zhang et al., 2011; Martius et al., 2016). Following Klawa and Ulbrich (2003) and Martius et al. (2016), we chose the 98th percentile, which is a compromise to capture the most extreme events in the CESM simulations while ensuring a sufficiently large sample size for robust statistical analysis. For model evaluation, which involves both the CESM model and ERA5 reanalyses (Figs. S1-S5 of the Supplement only), we use the 95th percentiles over the 1959-2019 period – such a lower threshold allows us for a more robust evaluation. The reason for this is that, given the ERA5's limited period, extremes in the reanalysis data set are more scarce and associated statistics for very extreme events are largely affected by sampling uncertainty (Bevacqua et al., 2021b). Selecting a slightly lower threshold allows us to reduce this sampling uncertainty and thus improve confidence in assessing the model's ability to simulate extremes (e.g., Bevacqua et al., 2021b; Kelder et al., 2022; Fischer et al., 2023).

2.2.2 Regional and spatially compounding effects of combined variability modes

To investigate the effect of variability modes on wintertime CWP extremes, we use three different metrics. The first metric allows for assessing the effect of modes in individual regions:

– **(Metric 1)** Regionally averaged counts of CWP extremes. Wintertime CWP counts are averaged by region over land-masses, weighted by the cosine of latitude to prevent overrepresentation of grid cells closer to the poles. This count-based metric allows us to assess the effects of variability modes on individual regions separately.

As Metric 1 is derived for each region individually, the influence of variability modes on the high regional frequencies of CWP extremes across multiple regions in the same winter (i.e., spatially compounding events) cannot be deduced directly. For example, based on Metric 1, we find that the variability mode phase ENSO+ modulates regionally averaged CWP extreme frequencies for North America and Central Asia. However, a possibility could be that half of the winter seasons with ENSO+ leads to increased CWP extremes for North America only, while the other half affects Central Asia, thus not simultaneously. Examining the dependencies between counts of CWP extremes in different regions can provide preliminary information on spatially compounding events (e.g., Bevacqua et al., 2021b) because regions connected by positive dependencies tend to experience CWP extremes at the same time. Thus, as a first step for investigating spatially compounding events, we analyse dependencies in Metric 1 computed for different regions, so as to provide preliminary information on groups of regions that may be affected by CWP extremes during the same winters.

Then, to examine spatially compounding events, we use two additional metrics. We employ these metrics to investigate the effects of variability modes on regional high frequencies of CWP extremes across multiple regions in the same winter (Metric 2) and on the total population of the Northern Hemisphere exposed to CWP extremes in the same winter (Metric 3).

– **(Metric 2)** Total number of affected regions during the same winter. For a given winter, a region is considered as affected by CWP extremes when the regionally averaged count of CWP extremes (Metric 1) is above its 80th percentile derived from the distribution of the 1950-2019 period. Then, similar to Singh et al. (2021), the total number of affected regions during the same winter is counted. Although choosing a higher percentile (>80th percentile) would enable us to focus on cases where regions are more severely affected, it would considerably limit the number of regions reported as affected and, consequently, the statistical robustness of our results.

– **(Metric 3)** Total population exposure. To assess the effects of variability modes on the population of the Northern Hemisphere exposed to CWP extremes during the same winter, we calculated for each winter the weighted averages of CWP extremes $wCWP$ (hereafter referred to as "population-weighted CWP extremes") using CWP extremes and population counts at the grid cell level as follows:

$$wCWP = \frac{\sum_{i=1}^{N_{grid}} N_{CWP_i} \times Pop_i}{\sum_{i=1}^{N_{grid}} Pop_i}$$

where N_{CWP_i} and Pop_i are the seasonal counts of CWP events and the population count at grid cell i, respectively, and N_{grid} is the total number of grid cells over the Northern Hemisphere. Population weighting is utilized here as a surrogate for the assets at risk that could experience damages due to CWP extremes (e.g., Bloomfield et al., 2023). For this purpose, global population counts for the year 2020 from the GPW product have been used (Columbia University, 2016).

In addition to enabling quantifying the number of affected regions depending on variability modes, Metric 2 is also used in Fig. 5b to assess the effect of the dependencies between regions on spatially compounding events. This analysis is performed by comparing the number of affected regions (i.e., Metric 2) from the original dataset with the number obtained after breaking the dependencies via randomly shuffling regional CWP extreme counts using bootstrap in all regions in time (Bevacqua et al., 2021a).

2.2.3   Identifying relevant effects of single and combined variability modes for the regional and spatial metrics

We quantify the effect of a positive (or negative) phase of a single variability mode of interest on wintertime CWP extremes based on the ratio between (i) CWP metrics under the positive (or negative) phase of the mode of interest, while additionally conditioning the other modes in a neutral state, and (ii) CWP metrics under all variability modes in neutral phase. Hereafter, we referred to this effect as *direct effect*. Following Singh et al. (2021), additionally conditioning all other modes in the neutral phase in (i) serves for better isolating the causal effects of the individual variability mode of interest. Specifically, such additional conditioning allows for taking into account confounding effects arising from the considered modes, still some confounding effects may remain. In particular, modes in neutral states still vary within the range of neutral conditions and we do not control for them. In addition; further effects may arise from variability mode not considered in this study. Similarly to the analysis of single variability modes, we quantify the effect of concurrent variability modes in non-neutral phases based

on the ratio between (i) CWP metrics under the concurrent modes of interest while conditioning all other modes to neutral conditions and (ii) CWP metrics under all variability modes in neutral phase. In terms of notation, we refer to concurrent climate variability modes by specifying (positive and negative) phases of NAO, PNA, ENSO and AMV in this order, with unspecified modes being in neutral states.

Although the main part of our study is based on the analysis of the metrics defined in subsection 2.2.2, we provide an overview of the direct (resp. combined) effects of modes on CWP extreme frequencies at the grid cell level in Fig. 2 (resp. Fig. 7). Results for the effects of variability modes on regionally averaged metric (Metric 1) and spatial metrics (Metrics 2 and 3) ratios are presented in Figs. 3, 4, and 6. For both regional and spatially compounding cases, we focus on the modes of variability influences leading to an enhancement in the means of the different metrics compared to neutral conditions (hereafter referred to as *positive effects*) – we focus on the increase, rather than the decrease, as this is of relevance for potential impact to society. This study does not investigate the influence of variability modes on the decrease of the metrics. When results for the different metrics are presented with box plots (Figs. 3, 5 and 6), the interquartile range and mean of the distribution are displayed.

Given the focus on four variability modes, each with three possible phases, there are eighty-one possible phase combinations, motivating the need for a synthesis of their effects. When presenting the results in Sect. 3, we focus our analysis on individual and concurrent variability modes having a *significant and positive* effect on the different metrics using permutation tests (see subsection 2.2.4 for more details on calculating the significance). To support the interpretation of the effects of concurrent variability modes on CWP metrics, in Figs. 3 and 6 we also show the effects of all univariate variability modes that contribute to the concurrent modes with significant effects regardless of whether they exert a significant effect in isolation compared to neutral conditions or not. Furthermore, to ensure robustness in the results, we disregard concurrent variability modes that occur very rarely by only considering concurrent variability modes with an empirical return period, defined as the inverse of their relative frequency, greater than 280 years (i.e., occurring for more than 10 years in our 2800 years dataset). It should be noted here that the empirical return periods for concurrent modes provided in this study are conditional as they are calculated by conditioning all other modes to neutral conditions. Therefore, such *conditional return periods*, despite providing an indication of the rarity of concurrent modes, should not be considered as absolute return periods as, by construction, they are larger than the unconditional return periods obtained without conditioning the other modes in neutral conditions. To provide an overview of the synthesis of the variability modes, effects of all possible concurrent modes are displayed for regionally averaged metric in Figs. S8-S14 (for a selection of regions for the sake of brevity) and spatial metrics in Fig. S15.

Finally, to provide insights into possible *amplified effects of concurrent variability modes* (Singh et al., 2021) relative to the effects of the modes that contribute to such combination, we identify combinations for which the average metric is higher than that of the *underlying mode sub-combinations* (note that no test here is performed, so this should be interpreted carefully, see explanations in subsection 2.2.4). For example, the concurrent modes NAO-PNA+ENSO+ are deemed to possibly have an amplified effect relative to the underlying mode sub-combinations if the average metric under NAO-PNA+ENSO+ is higher than the underlying mode sub-combinations, which are NAO-, PNA+ and ENSO+ taken in isolation, as well as the bivariate

8

mode sub-combinations NAO-PNA+, NAO-ENSO+ and PNA+ENSO+. The identified combinations with amplified effects are highlighted in Figs. 3, 4, 6 and 7 via dark blue box plots and boxes.

2.2.4 Permutation test procedure to assess significance in effects of combined variability modes

As already mentioned in subsection 2.2.3, the statistical significance of the effects of individual and concurrent variability modes on CWP metrics compared to neutral conditions is assessed using permutation tests (e.g., Bradley, 1968; Good, 2013; DelSole et al., 2017; Singh et al., 2021). Specifically, for a given CWP metric, we test whether the ratio of the average of the metric associated with a given set of phases of interest (e.g., NAO+ENSO-, set as the numerator) to the average of the metric under neutral conditions (set a denominator) is larger than one at significance level $\alpha = 0.10$ based on one-sided tests. Compared to a lower significance level, our chosen level allows the detection of significant effects of modes of variability while reducing false negatives in the context of small sample sizes. To test the hypothesis that the average of the metric under individual and concurrent variability modes is higher than under neutral conditions, we compared the ratio obtained from the original samples with a confidence interval of the ratio obtained from data without an effect of the modes on the CWP metric. Specifically, the latter was obtained via randomly permuting without replacement the samples for both numerator and denominator, and re-estimate the ratio from the resampled data. By repeating this procedure, we can then define a confidence interval for the ratio and a critical region for test rejection. If the original ratio is higher than the $(1 - \alpha) * 100$th percentile, the average of the metric associated with the set of phases of interest is considered to be significantly higher than that of the neutral conditions. As several tests are carried out for the different concurrent modes, a Bonferroni correction (e.g., Bonferroni, 1936; Sedgwick, 2014) is applied to control the overall probability of Type I (or false positive) errors. Please note that, while identifying concurrent variability modes with significantly *amplified* effects relative to the effects of the modes that contribute to such combination is relevant, it has not been done in this study as no statistically consistent procedure including Bonferroni correction has been found for such a statistical problem. For example, to identify the concurrent modes NAO+ENSO+AMV+ as having a significantly amplified effect on the metrics, six permutation tests comparing the effects of NAO+ENSO+AMV+ against those of its six sub-combinations must all reject the equality of effects. Designing such a statistical test procedure while controlling the false discovery rate goes beyond the scope of the present study and is therefore not included in the analysis. In addition, in Figs. 2 and 7 only, we assess whether averages of the CWP extreme frequencies at the grid cell level associated with a given set of phases are significantly different compared to neutral conditions (i.e., not necessarily larger). For these tests performed at the grid cell level, we use two-sided permutation tests. In this case, the critical region for rejection is defined using the $(\frac{\alpha}{2}) \times 100$th and $(1 - \frac{\alpha}{2}) \times 100$th percentiles.

Regarding the number of samples m for permutation tests, several trials showed that choosing $m = 100,000$ allows us to obtain robust results for the three different metrics. Thus, the analysis of the three metrics was carried out using $m = 100,000$. However, when applied to the grid cell level for Figs. 2 and 7, results from permutation tests proved less sensitive to the choice of the number of sample, and m was chosen to be equal to 100.

3 Results

Before investigating the effect of individual variability modes and concurrent modes on CWP extremes and associated spatially compounding events in CESM simulations for the 1950-2019 period, we carried out a model evaluation with respect to ERA5 over the 1959-2019 period. Such a model evaluation is mainly performed for the effects of individual variability modes, as a robust assessment of the effects of concurrent variability modes requires a large sample size (Singh et al., 2021). For the same reason, the effects of individual variability modes in ERA5 are evaluated without constraining the other modes to be in the neutral phase (which thus differs from the *direct effects* of variability modes defined in subsection 2.2.3).

Results for model evaluation are displayed in Figs. S1-S5 of the Supplement. Although the simulated CWP absolute frequencies exhibit some biases with respect to ERA5 over the Northern Hemisphere (Fig. S1), CESM provides an adequate representation of the anomalies in CWP frequencies induced by individual variability modes relative to neutral conditions (Figs. S2-S5). We conclude from this model evaluation that CESM is suitable for further investigating the CWP extremes and their relationships with variability modes. In the following, we assess the effect of modes of variability and their combinations on CWP extremes via the CESM model based on the 98th percentiles, and also provide a one-to-one comparison with ERA5 based on the same percentiles.

3.1 Direct effects of variability modes on regional CWP extremes

Examining the direct effects of variability modes on CWP extremes in CESM simulations (Fig. 2) shows that different phases of NAO, PNA and ENSO significantly modulate CWP extreme frequencies over multiple regions of the Northern Hemisphere. Within Europe, NAO+ and NAO- significantly increase CWP extremes in Northern Europe (NEU) and the Mediterranean region (MED), respectively (Figs. 2a and 2b). NAO+ also significantly influences CWP extremes in the Russian-Arctic (RAR) and Western Siberia (WSB). The low pressure associated with storms under NAO+ is accurately represented in CESM simulations (Fig. S6a), with negative pressure anomalies partially or fully covering the regions experiencing a significant increase in CWP extremes. An exception to such CWP enhancement associated with low pressure is found for Northeastern North America (NEN) during NAO-, where high sea level pressure anomalies of $\sim +3$ hPa are associated with increased CWP extremes. While no regions experience increased CWP extremes under PNA+ (Fig. 2c), PNA- significantly increases CWP extremes compared with neutral conditions in Eastern Siberia (ESB) and Russian Far East (RFE) within North Asia (Fig. 2d), and in Northeastern North America (NEN), Northwestern North America (NWN) and Western North America (WNA) in the North America macroarea.

Among the oceanic modes of variability ENSO and AMV, the former has the most relevant and widespread effects. ENSO+ (Fig. 2e) increases CWP extremes across three regions of Africa (Arabian Peninsula ARP, Sahara SAH and Western Africa WAF). For ENSO- (Fig. 2f), CWP extremes are significantly increased for two regions within Central-South Asia: South Asia (SAS) and East Asia (EAS). For the AMV, we find no significant regional effects of AMV+ and AMV- conditions (Figs. 2g and 2h), in line with weak sea level pressure anomalies associated with AMV phases, ranging from ~ -1.5 to $\sim +1.5$ hPa (Figs. S6g and S6h).

3.2 Effects of concurrent anomalies in variability modes on regional CWP extremes

Model simulations (CESM) show that not only individual variability modes can have effects on regional wintertime frequencies of CWP extremes, but also combinations of modes (Fig. 3; Fig. S7 shows the same but for absolute frequencies). Figure 4 provides a summary of these effects, including the count of modes combinations that enhance CWP extremes compared to neutral conditions for each region. For example, Northern Europe (NEU) exhibits the highest count of mode combinations that significantly enhance CWP extreme frequencies compared to neutral conditions, with eleven mode combinations that all involve NAO+. The presence of a given mode phase or combination of mode phases that has an effect on CWP extremes in multiple regions suggests the potential for spatially compounding events, which will be examined in subsection 3.3. In the following, we focus on describing the effects of a selection of mode combinations and regions in Figs. 3-5. To maintain clarity and conciseness, we do not discuss all regions and mode combinations in the text, and readers can explore specific regional effects directly in the figures.

For the Mediterranean region (MED) in Europe (Fig. 3a), five concurrent variability modes containing NAO- have significant positive effects with respect to neutral conditions. Among these five concurrent variability modes, three combinations of modes have an amplified effect relative to the underlying mode sub-combinations (blue boxes). For example, in the MED region, CWP extremes are on average ~ 1.5 times more likely under the concurrent mode NAO-ENSO+ than under neutral conditions, while being ~ 1.1 and ~ 1.2 times more likely than under NAO- and ENSO+ in isolation, respectively. Note that the conditional empirical return period of NAO-ENSO+ (i.e., conditioning all other modes to neutral conditions) is 65 years, while it is equal to 20 and 30 years for NAO- and ENSO+, respectively, which means that the concurrent mode NAO-ENSO+ (with other modes being in neutral conditions) is ~ 3 and ~ 2 times less likely to occur in any given year than NAO- or ENSO+ in isolation (with other modes being in neutral conditions).

Concurrent modes can also amplify CWP extreme frequencies in other regions. For example, in the Arabian Peninsula (ARP) within Africa, CWP extremes are on average ~ 3.5 times more likely than neutral conditions under ENSO+. However, when ENSO+ combines with NAO-PNA+, CWP extremes are on average ~ 4 times more likely, while both individual modes (NAO- and PNA+) do not have a significant effect on the mean frequency of CWP extreme frequencies relative to neutral conditions. Interestingly, the combination of NAO-ENSO+ has an amplified effect relative to the underlying mode sub-combinations in all three African regions, increasing approximately the likelihood of CWP extremes frequencies by a factor of ~ 4, 1.5 and 2 relative to neutral conditions in the Arabian Peninsula (ARP), Sahara (SAH) and Western Africa (WAF), respectively.

The Central North America (CNA) region illustrates how the effects of individual modes can combine to significantly increase CWP extreme frequencies in a given winter relative to neutral conditions, even if individual modes do not exert significant effects in isolation. For example, despite the fact that both PNA+ and ENSO+ in isolation do not significantly increase CWP extremes (indicated by no grey arrows in Fig. 3b), combined PNA+ENSO+ increases significantly the likelihood of CWP extremes by a factor of ~ 1.5 compared to neutral conditions (indicated by the grey arrow and blue box). Furthermore, within North America, the region with the most combinations of modes that present amplified effects on CWP extreme frequencies is

340 East North America (ENA), with six separate combinations (see blue boxes). Of these combinations, ENSO is always in the positive phase, indicating its potentially large effect on CWP extremes.

In North Asia, concurrent variability modes increase CWP extreme frequencies by ~ 1.5 to ~ 2 times relative to neutral conditions depending on the combination. In particular, PNA-ENSO- increases CWP extreme frequencies by ~ 1.5 times in three of North Asia's four regions (Eastern Siberia ESB, Russian-Arctic RAR and Russian Far East RFE).

345 Within Central South Asia, the Tibetan-Plateau (TIB) exemplifies again how individual modes without significant effects on CWP extremes (here, AMV- and ENSO+) can combine to significantly increase the likelihood of CWP extremes during winters. Across the five regions of Central South Asia, all concurrent modes that, on average, led to more CWP extremes than their underlying mode sub-combinations (blue boxes) include the variability mode ENSO. Of these concurrent modes, ENSO is always in the positive phase within the inland regions (ECA, TIB and WCA); while being in the negative phase in the coastal
350 regions (EAS and SAS).

Regarding the comparison of CESM results with those of ERA5, the range of CESM ratios of regionally averaged CWP extreme frequencies with respect to neutral conditions generally covers the values for ERA5 for the different concurrent modes, when available (Fig. 3).

Results from Fig. 3 and the summary in Fig. 4 cannot be used to conclude whether the effects of concurrent variability modes
355 lead to spatially compounding CWP extremes, that is, to high wintertime frequencies of CWP extreme across multiple regions during the same winter. These figures illustrate the effect of individual and concurrent variability modes on regionally averaged CWP extreme frequencies, which are derived for each region separately. Nevertheless, the number of regions where each mode combination has significant effects in Fig. 4 (see numbers on the top of the matrix) suggests that some mode combinations may potentially lead to spatially compounding CWP extremes. For example, NAO-ENSO+ significantly enhances regional CWP
360 extreme frequencies in eight regions, which means that if these regional effects of NAO-ENSO+ can manifest in the same winter, NAO-ENSO+ would lead to spatially compounding CWP extremes. In the next section, we assess whether individual and concurrent variability modes can lead to concurrent CWP extremes during the same winters across regions.

3.3 Effects of concurrent variability modes on spatially compounding CWP extremes

As the first step in the investigation of spatially compounding events, we examine dependencies between counts of CWP
365 extremes in different regions, which provides preliminary information on groups of regions that may be affected by CWP extremes during the same winters. Figure 5a shows Spearman correlations of regionally averaged CWP extreme frequencies (Metric 1) between all pairs of regions. Regions that are geographically close tend to be positively correlated (see correlation values in contoured black boxes), in line with spatial autocorrelation. However, also some regions that are from different macroareas and therefore more distant can be correlated, e.g., Central-South Asian regions with African regions or North
370 American regions with North Asian regions. This highlights the potential for underlying effects of modes of variability that can connect distant regions. Notably, Fig. 5a highlights that most of the pair correlations between CWP extreme counts in different regions are positive.

12

In line with such dominant positive correlations (Fig. 5a), we find that dependencies among regions overall enhance the potential for spatially compounding events. Specifically, the distribution of the number of regions affected during the same winters (Metric 2) is different from that obtained by assuming independence between regions (Fig. 5b), with dependencies elongating both tails of the distribution. For spatially compounding extremes on the right tail of the distribution, this implies a higher 50-year return level for the number of regions affected by high CWP counts in the same winter compared to independence, that is 11 instead of 9 affected regions (see vertical lines). Consistent with findings in Bevacqua et al. (2021a), this dependency-driven shift is not observed for the mean of the distribution (not shown).

The increased count of regions under CWP extremes due to the dependencies among regions can be linked to modes of variability. That is, the high number of regions simultaneously affected by CWP extremes, which is possible due to the dependencies among regional CWP extremes, would also not be possible without the effects of concurrent variability modes (Fig. 5c). In particular, when all variability modes are neutral, on average around four regions are affected simultaneously by high regionally averaged CWP extremes. Generally, as the number of variability modes in anomalous conditions increases, the likelihood of multiple regions simultaneously experiencing extreme conditions also increases (Fig 5c; see letters indicating significant differences among distributions, with the exception of the distributions related to three and four modes). Notably, this effect is even more marked when focusing on winter seasons with an extreme number of regions affected (right whiskers of the boxplots). Overall, these results indicate that concurrent anomalies in variability modes are key for spatially compounding events.

Given the dependencies among regions and that combinations of variability modes are essential for spatially compounding CWP extremes, we move to identify which are the relevant mode combinations that enhance the number of regions affected by CWP extremes (Metric 2) and population exposed to CWP extremes (Metric 3). We find that thirteen individual and concurrent variability modes significantly increase the number of affected regions compared to neutral conditions (Fig. 6a). Three bivariate combinations have a significant effect on the total number of affected regions and an amplified effect relative to their underlying mode sub-combinations (see blue boxes for ENSO+AMV-, PNA+ENSO+ and NAO-ENSO+). NAO-ENSO+ nearly doubles the number of regions simultaneously exposed to CWP extremes on average relative to neutral conditions.

In terms of population exposed to CWP extremes, four combinations (ENSO-AMV+, NAO-PNA+ENSO+, NAO+ENSO-AMV+ and PNA-ENSO-) are identified as having a significant effect compared to neutral conditions (Fig. 6b). Among these four combinations, only one (NAO-PNA+ENSO+) has already been identified as having a significant effect on the number of affected regions in Fig. 6a. It highlights that the heterogeneous distribution of population density across regions needs to be considered to assess the societal vulnerability to CWP extremes. In particular, variability modes in isolation do not lead to significant effects on the population exposure compared to neutral conditions (Fig. 6b), indicating the importance of considering combinations of modes to distil the effects of modes of variability on the population affected. Notably, while ENSO+ dominates the influence of modes of variability on the number of affected regions (see "+" sign in Fig. 6a), ENSO- dominates for the population affected (see "−" sign in Fig. 6b).

3.4 Physical mechanisms underlying spatially compounding CWP extremes

We now move to inspect the physical mechanisms leading to spatial co-occurrences of CWP extremes by analysing SLP anomalies for concurrent variability modes with significant effects on spatially compounding events (Fig. 7). Here, negative SLP anomalies during winter are generally considered indicative of storminess, a key driver of CWP extremes. In the analysis, we restrict to the seven combinations having an amplified effect relative to their underlying mode sub-combinations on Metric 2 and Metric 3 (i.e. combinations with blue boxes in Fig. 6): namely, NAO-ENSO+, PNA+ENSO+ and ENSO+AMV- for affected regions (Fig. 6a) and PNA-ENSO-, ENSO-AMV+, NAO+ENSO-AMV+ and NAO-PNA+ENSO+ for exposed population (Fig. 6b). These combinations have a reasonably low conditional return period (≤ 82 years; see Methods), thus are not very unlikely events in the model simulations.

The largest positive effects on the number of affected regions (Fig. 6a) occurs under concurrent ENSO+ (El Niño phase) and NAO-, that is NAO-ENSO+ (Figs. 7a and 7b). Under such a combination of modes of variability NAO-ENSO+, negative SLP anomalies patterns intensify and expand over the North Atlantic Ocean compared to those for modes NAO- and ENSO+ in isolation (Figs. S6b and S6e), in line with the enhancement of CWP extremes over many regions of North America, North Central America, Europe and Africa.

Although the combination of modes PNA+ENSO+ has smaller significant positive effects on the number of affected regions than that of NAO-ENSO+ (Fig. 6a), PNA+ENSO+ may be more frequent than NAO-ENSO+ (given their lower conditional return period; see Methods). Such a PNA+ENSO+ combination (Figs. 7c and 7d) intensifies the negative SLP anomalies patterns on both sides of North America with respect to PNA+ and ENSO+ modes in isolation (Figs. S6c and S6e). This is consistent with the amplification of CWP extreme frequencies for regions within North America, Central America and Africa. In contrast, when ENSO+ combines with AMV- (ENSO+AMV-; Figs. 7e and 7f), negative SLP anomalies patterns are quite similar to those of ENSO+ in isolation (Fig. S6e); this suggests that AMV- has a limited amplifying effect on CWP extremes, in line with Fig. 6a.

Under the resulting combination PNA-ENSO- (Figs. 7g and 7h), which shows the largest positive effects on the population exposure (Fig. 6b), negative SLP anomalies are intensified over North Asian region, compared to those for modes in isolation (Figs. S6d and S6f). These intensified low-pressure conditions associated with storminess increase CWP extreme frequencies over a number of densely populated regions in North Asia and East Asia. PNA-ENSO- exemplifies how combined variability modes can lead to spatially compounding events by adding up the effects of individual modes in isolation. Specifically, under PNA-ENSO- the population exposed to extreme CWP extremes under PNA- and ENSO- in isolation partially adds up, resulting in spatially compounding events with a large population affected by CWP extremes.

Although the effects of combined variability modes ENSO-AMV+ (Figs. 7i and 7j) are rather limited, when combined with NAO+ (NAO+ENSO-AMV+; Figs. 7k and 7l) negative SLP anomalies are intensified over high latitudes, mainly due to NAO+ influence (Fig. S6a) and over South Asia, due to ENSO- (Fig. S6f). These intensified low-pressure systems lead to an amplification of CWP extremes in Northern Europe and South Asia. It is interesting to note that these two regions are not the same affected by ENSO-AMV+ (Figs. 7i-j), suggesting a strong influence of the NAO on regions impacted by CWP extremes.

14

440   Similar to what is observed for NAO-ENSO+, NAO-PNA+ENSO+ features a negative SLP anomaly extending across the Southern North Atlantic (Fig. 7n). However, for some regions, the addition of PNA+ to NAO-ENSO+ tends to weaken the effects of concurrent variability modes on CWP extremes, as some regions exhibit, on average, fewer regional CWP extremes than those obtained under NAO-ENSO+ (see blue boxes in Figs. 7n and 7m).

4   Discussion

445 Several results regarding the direct effects of variability modes on CWP extremes in CESM simulations (subsection 3.1) align with well-established findings in the literature, thereby validating the robustness of CESM modeling. Table S1 provides a concise summary of the agreement between CESM simulations and existing literature. Among these results are the influence of the NAO+ regime favoring CWP extremes in Northern Europe due to stronger than average westerly winds (e.g., Hurrell and Deser, 2010), or the influence of PNA- favoring blocking in the Pacific (e.g., Li et al., 2017), increasing storm frequency in the
450 Northern Pacific. However, several results lack direct support from existing literature. While they may represent novel findings, they should be interpreted cautiously, considering the biases of CESM simulations relative to ERA5. Notably, the direct effect of ENSO+ on CWP extreme frequencies in CESM simulations exhibits some inconsistencies when compared to ERA5 over Northern Africa (Fig. S3). Better understanding and confirming the influence of climate modes on arid regions (e.g., Northern Africa), where CWP events may be less intense than in other areas, can support adaptation and mitigation policies. While CWP
455 extremes can serve as an important source of freshwater (e.g., Berdugo et al., 2020), they also present a significant flood risk (e.g., Yin et al., 2023).

     We analysed event counts aggregated over winter and at the scale of predefined SREX regions, given that high counts of compound extremes at these scales are expected to have negative effects on society. While the 98th percentile has been used in this study to focus on extremes and is relatively well-established in the literature (e.g., Klawa and Ulbrich, 2003; Martius
460 et al., 2016), other higher thresholds could have been chosen to consider more intense extreme events (e.g., Liu et al., 2013; Schär et al., 2016; Camuffo et al., 2020). Figs. S16-S19 show results from a sensitivity analysis on the influence of variability modes on regional CWP extremes (Metric 1) and spatially compounding events (Metrics 2 and 3) with the 99th and 99.5th percentiles used as thresholds. Although there are some variations in the results compared to those for the 98th percentile, the main conclusions drawn across the different thresholds are broadly consistent for all Metrics. The magnitude of the effects of
465 the combinations are generally consistent across thresholds, and the combinations detected at higher thresholds are generally included among those identified at lower thresholds (Figs. S16-S19). Such slight differences may be due to larger sampling uncertainty for higher thresholds limiting the ability to detect significant effects for higher thresholds rather than different physical mechanisms involved for different thresholds. While the sensitivity analyses broadly indicate the robustness of most of our findings, possible relevant differences across thresholds highlight the importance of identifying impact-relevant thresholds,
470 though this task is challenging (e.g., Williams, 1978; Bloomfield et al., 2023). In addition, the selected SREX regions may not reflect the natural spatial patterns of variation of CWP extremes, potentially occurring at a more localized scale or span across multiple regions. We also note that variability modes such as AMV or ENSO can have lagged effects on regional climate

extremes (e.g., Ruiz-Barradas et al., 2000; Wang, 2019; Xing et al., 2022), an aspect that has been partially taken into account in this study for ENSO. Furthermore, additional variability modes than those considered here (e.g., the Indian Ocean Dipole (IOD), Chongyin and Mingquan, 2001; Qiu et al., 2014; Kurniadi et al., 2021) may be related to CWP frequencies in some regions, especially in the regions where the different combinations of the variability modes NAO, ENSO, PNA and AMV had no significant effects (in Fig. 3). In addition, the IOD is known to co-vary with some of the modes examined here, e.g. with ENSO and the AMV (e.g., Ashok et al., 2003; Stuecker et al., 2017; Xue et al., 2022). Overall, although our aggregation in time and space may not be optimal for providing a fine-grained analysis of CWP events and additional modes may be relevant in some regions, this study provides a first comprehensive assessment of the interactions between multiple climate variability modes and the frequency of wintertime CWP extremes and associated spatially compounding events across regions of the Northern Hemisphere. In particular, analyzing spatially compound events highlights the potential influence of variability modes that can link distant regions. These long-range relationships modulated by mode combinations can be explored in more detail, for example, with tailored experiments such as nudged atmospheric simulations.

We mainly focused on the increase in the frequency of CWP extremes, however we note that increases in intensity at the same frequency, as well as low frequencies of CWP extremes may also be relevant information for the insurance industry (e.g., Ciullo et al., 2023). Studying the influence of variability modes on the intensity of the drivers (here, wind and precipitation) could further support mitigation and adaptation strategies (e.g., Whan and Zwiers, 2017; Li et al., 2022). Quantifying these effects on wind and precipitation in isolation would allow for a decomposition of the effects of concurrent variability modes, giving an even more complete picture of the processes involved (e.g., Manning et al., 2018; Brunner et al., 2021; Calafat et al., 2022). In addition, regarding spatial metrics, considering other relevant measures that combine return period information with the exposed population would allow for focusing on concurrent variability modes that regularly expose the population to CWP extremes.

With the methodology used here, it is not possible to thoroughly examine the causality behind the dependence between different variability modes and between the modes and CWP extremes. It is however clear that there exist important interactions and causal links between oceanic and atmospheric variability modes at different time scales, e.g., between ENSO and the NAO (e.g., Kirov and Georgieva, 2002; Deser et al., 2017; Yeh et al., 2018), between the AMV and the NAO (e.g., Hurrell and Deser, 2010; Fang et al., 2018) and between ENSO and the PNA (Renwick and Wallace, 1996). Therefore, these modes are dependent on each other, a relevant information to take into account when investigating the causal effects of climate variability modes on characteristics of spatially compounding events. Applying statistical methods such as regression techniques (e.g., Pearl, 2013; Kretschmer et al., 2021), or more advanced approaches such as causal networks (e.g., Nowack et al., 2020) may help to shed light on the complete causal pathway leading to spatially compounding events and better control potential confounding effects. We also note that dependencies among modes influence the return periods of concurrent modes, that is, certain signs of modes will co-occur with others more frequently than others, such as e.g. ENSO+NAO-, with an effect on their associated CWP extreme frequencies. In line with heterogeneous dependencies among different modes, we estimated a wide range of return periods for the different mode combinations (Fig. 3).

A natural continuation of this work is the application of the methodology developed in this study to investigate 1) the influence of climate modes on CWP extremes in the Southern Hemisphere, 2) summertime CWP extremes and 3) changes in CWP extremes over time, as well as their spatial relationships and dependencies with climate variability modes under climate change (Bevacqua et al., 2023).

5 Conclusions

In this study, we present the first comprehensive assessment of the relation between individual and concurrent climate variability modes and the frequency of wintertime CWP extremes and associated spatially compounding events across regions of the Northern Hemisphere using CESM simulations. We show that simulated concurrent modes are associated with an amplification of CWP extreme frequencies in many individual regions compared to variability modes in isolation. We have identified groups of regions with positive spatial correlations between regional wintertime CWP extremes. These correlations enable extreme spatially compounding events with many regions experiencing CWP extremes during the same winter. We found that such extreme spatially compounding events, which also include a large fraction of the population of the Northern Hemisphere under CWP extremes in the same winter, are possible due to the combinations of multiple variability modes in anomalous phases and their influence on the atmospheric circulation. For example, the combination of ENSO- and NAO+ nearly double the number of affected regions compared to neutral conditions on average. Among the modes, ENSO is found to be the most influential variability responsible for spatially compounding extreme events, which aligns with its known effects on weather and climate extremes worldwide (Goddard and Gershunov, 2020). The high return periods associated with some of the concurrent modes that lead to extreme spatially compounding events make it potentially difficult to factor these findings into long-term planning, e.g., infrastructure development or (re)insurance modelling. However, by identifying the drivers of the most extreme events, the findings raise awareness on the potential for extreme compounding events under certain mode combinations, which could be factored into weekly, sub-seasonal (White et al., 2022), seasonal (Lenssen et al., 2020) and longer forecasts to better anticipate mitigation action and climate services (Osman et al., 2023).

By using two different metrics to characterise spatially compounding events, we highlight that the effects of concurrent variability modes can differ from one spatial metric to another. While combinations with ENSO+ lead to the largest number of affected regions, when weighted by population exposure, combinations with ENSO- lead to higher effects on population. Our analysis thus stresses the importance of considering not only the interplay between variability modes but also a careful choice of metrics, which should be tailored to the ultimate impacts of interest, so as to assess the relevant characteristics of spatially compounding events and improve their risk management and mitigation.

semble Community Project website: https://www.earthsystemgrid.org/dataset/ucar.cgd.ccsm4.CLIVAR_LE.html. Modes of variability for CESM can be accessed via the CVDP-LE Data Repository https://www.cesm.ucar.edu/projects/cvdp-le/data-repository.

References

Abeysirigunawardena, D. S., Gilleland, E., Bronaugh, D., and Wong, P.: Extreme wind regime responses to climate variability and change in the inner south coast of British Columbia, Canada, Atmosphere-Ocean, 47, 41–62, https://doi.org/10.3137/AO1003.2009, 2009.

Ashok, K., Guan, Z., and Yamagata, T.: A Look at the Relationship between the ENSO and the Indian Ocean Dipole, Journal of the Meteorological Society of Japan. Ser. II, 81, 41–56, https://doi.org/10.2151/jmsj.81.41, 2003.

Berdugo, M., Delgado-Baquerizo, M., Soliveres, S., Hernández-Clemente, R., Zhao, Y., Gaitán, J. J., Gross, N., Saiz, H., Maire, V., Lehmann, A., Rillig, M. C., Solé, R. V., and Maestre, F. T.: Global ecosystem thresholds driven by aridity, Science, 367, 787–790, 2020.

Bevacqua, E., De Michele, C., Manning, C., Couasnon, A., Ribeiro, A. F. S., Ramos, A. M., Vignotto, E., Bastos, A., Blesić, S., Durante, F., Hillier, J., Oliveira, S. C., Pinto, J. G., Ragno, E., Rivoire, P., Saunders, K., van der Wiel, K., Wu, W., Zhang, T., and Zscheischler, J.: Guidelines for Studying Diverse Types of Compound Weather and Climate Events, Earth's Future, 9, e2021EF002 340, https://doi.org/10.1029/2021EF002340, e2021EF002340 2021EF002340, 2021a.

Bevacqua, E., Shepherd, T. G., Watson, P. A. G., Sparrow, S., Wallom, D., and Mitchell, D.: Larger Spatial Footprint of Wintertime Total Precipitation Extremes in a Warmer Climate, Geophysical Research Letters, 48, e2020GL091 990, https://doi.org/10.1029/2020GL091990, e2020GL091990 2020GL091990, 2021b.

Bevacqua, E., Zappa, G., Lehner, F., and Zscheischler, J.: Precipitation trends determine future occurrences of compound hot–dry events, Nat. Clim. Chang., https://doi.org/10.1038/s41558-022-01309-5, 2022.

Bevacqua, E., Suarez-Gutierrez, L., Jézéquel, A., Lehner, F., Vrac, M., Yiou, P., and Zscheischler, J.: Advancing research on compound weather and climate events via large ensemble model simulations, Nature Communications, 14, 2145, https://doi.org/10.1038/s41467-023-37847-5, 2023.

Bevacqua, E., Rakovec, O., Schumacher, D. L., Kumar, R., Thober, S., Samaniego, L., Seneviratne, S. I., and Zscheischler, J.: Direct and lagged climate change effects intensified the 2022 European drought, Nature Geoscience, 17, 1100–1107, 2024.

Blocken, B. and Carmeliet, J.: A review of wind-driven rain research in building science, Journal of Wind Engineering and Industrial Aerodynamics, 92, 1079–1130, https://doi.org/https://doi.org/10.1016/j.jweia.2004.06.003, 2004.

Bloomfield, H., J., H., A., G., A.L., K., L.C., S., F., P., R., J., D., K., A., C., and P.D., B.: Co-occurring wintertime flooding and extreme wind over Europe, from daily to seasonal timescales, Weather and Climate Extremes, 39, 100 550, https://doi.org/https://doi.org/10.1016/j.wace.2023.100550, 2023.

Bloomfield, H. C., Bates, P., Shaffrey, L. C., Hillier, J., Champion, A., Cotterill, D., Pope, J. O., and Kumar, D.: Synoptic conditions conducive for compound wind-flood events in Great Britain in present and future climates, Environmental Research Letters, 19, 024 019, https://doi.org/10.1088/1748-9326/ad1cb7, 2024.

Bonferroni, C.: Teoria Statistica Delle Classi e Calcolo Delle Probabilita, Pubblicazioni del R Istituto Superiore di Scienze Economiche e Commerciali di Firenze (Libreria Internazionale Seeber, Florence, Italy), 8, 3–62, 1936.

Bradley, J. V.: Distribution-Free Statistical Tests, pp. 283–310, 1968.

Brunner, M. I., Swain, D. L., Gilleland, E., and Wood, A. W.: Increasing importance of temperature as a contributor to the spatial extent of streamflow drought, Environ. Res. Lett., 16, 024 038, https://doi.org/10.1088/1748-9326/abd2f0, 2021.

Calafat, F. M., Wahl, T., Tadesse, M. G., and Sparrow, S. N.: Trends in Europe storm surge extremes match the rate of sea-level rise, Nature, 603, 841–845, https://doi.org/10.1038/s41586-022-04426-5, 2022.

590 Camberlin, P., Janicot, S., and Poccard, I.: Seasonality and atmospheric dynamics of the teleconnection between African rainfall and tropical sea-surface temperature: Atlantic vs. ENSO, International Journal of Climatology, 21, 973–1005, https://doi.org/https://doi.org/10.1002/joc.673, 2001.

Camuffo, D., Becherini, F., and della Valle, A.: Relationship between selected percentiles and return periods of extreme events, Acta Geophysica, 68, 1201–1211, https://doi.org/10.1007/s11600-020-00452-x, 2020.

595 Cerveny, R. S. and Newman, L. E.: Climatological Relationships between Tropical Cyclones and Rainfall, Monthly Weather Review, 128, 3329 – 3336, https://doi.org/10.1175/1520-0493(2000)128<3329:CRBTCA>2.0.CO;2, 2000.

Chongyin, L. and Mingquan, M.: The Influence of the Indian Ocean Dipole on Atmospheric Circulation and Climate, Advances in Atmospheric Sciences, 18, 831–843, https://doi.org/10.1007/BF03403506, 2001.

Ciullo, A., Strobl, E., Meiler, S., Martius, O., and Bresch, D. N.: Increasing countries' financial resilience through global catastrophe risk
600 pooling, Nature Communications, 14, 922, https://doi.org/10.1038/s41467-023-36539-4, 2023.

Coles, S., Heffernan, J., and Tawn, J.: Dependence Measures for Extreme Value Analyses, Extremes, 2, 339–365, https://doi.org/10.1023/A:1009963131610, 1999.

Columbia University, C. f. I. E. S. I. N. . C.: Gridded Population of the World, Version 4 (GPWv4): Population Density, https://doi.org/10.7927/H4NP22DQ, 2016.

605 Davini, P., Hardenberg, J., and Corti, S.: Tropical origin for the impacts of the Atlantic Multidecadal Variability on the Euro-Atlantic climate, Environmental Research Letters, 10, 094 010, https://doi.org/10.1088/1748-9326/10/9/094010, 2015.

DelSole, T., Trenary, L., Tippett, M. K., and Pegion, K.: Predictability of Week-3–4 Average Temperature and Precipitation over the Contiguous United States, Journal of Climate, 30, 3499 – 3512, https://doi.org/10.1175/JCLI-D-16-0567.1, 2017.

Deser, C., Simpson, I. R., McKinnon, K. A., and Phillips, A. S.: The Northern Hemisphere Extratropical Atmospheric Circulation Re-
610 sponse to ENSO: How Well Do We Know It and How Do We Evaluate Models Accordingly?, Journal of Climate, 30, 5059 – 5082, https://doi.org/10.1175/JCLI-D-16-0844.1, 2017.

Domeisen, D. I., Garfinkel, C. I., and Butler, A. H.: The teleconnection of El Niño Southern Oscillation to the stratosphere, Reviews of Geophysics, 57, 5–47, 2019.

Dowdy, A. and Catto, J.: Extreme weather caused by concurrent cyclone, front and thunderstorm occurrences, Scientific Reports, 7, 40 359,
615 https://doi.org/10.1038/srep40359, 2017.

Elsner, J. B., Bossak, B. H., and Niu, X.-F.: Secular changes to the ENSO-U.S. hurricane relationship, Geophysical Research Letters, 28, 4123–4126, https://doi.org/https://doi.org/10.1029/2001GL013669, 2001.

Fang, K., Chen, D., Ilvonen, L., Frank, D., Pasanen, L., Holmström, L., Zhao, Y., Zhang, P., and Seppä, H.: Time-varying relationships among oceanic and atmospheric modes: A turning point at around 1940, Quaternary International, 487, 12–25,
620 https://doi.org/10.1016/j.quaint.2017.09.005, asia Pacific 2K, 2018.

Fischer, E. M., Beyerle, U., Bloin-Wibe, L., Gessner, C., Humphrey, V., Lehner, F., Pendergrass, A. G., Sippel, S., Zeder, J., and Knutti, R.: Storylines for unprecedented heatwaves based on ensemble boosting, Nature Communications, 14, 4643, https://doi.org/10.1038/s41467-023-40112-4, 2023.

Foulds, S. and Warburton, J.: Significance of wind-driven rain (wind-splash) in the erosion of blanket peat, Geomorphology, 83, 183–192,
625 https://doi.org/10.1016/j.geomorph.2006.07.001, 2007.

Gampe, D., Schwingshackl, C., Böhnisch, A., Mittermeier, M., Sandstad, M., and Wood, R. R.: Applying global warming levels of emergence to highlight the increasing population exposure to temperature and precipitation extremes, Earth System Dynamics, 15, 589–605, https://doi.org/10.5194/esd-15-589-2024, 2024.

Gao, T., Xu, Y., Wang, H. J., Sun, Q., Xie, L., and Cao, F.: Combined Impacts of Climate Variability Modes on Seasonal Precipitation Extremes Over China, Water Resources Management, 36, 2411–2431, https://doi.org/10.1007/s11269-022-03150-z, 2022.

Goddard, L. and Gershunov, A.: Impact of El Niño on weather and climate extremes, El Niño Southern Oscillation in a changing climate, pp. 361–375, 2020.

Good, P.: Permutation Tests: A Practical Guide to Resampling Methods for Testing Hypotheses, Springer Science & Business Media, 2013.

Greeves, C., Pope, V., Stratton, R., and Martin, G.: Representation of Northern Hemisphere winter storm tracks in climate models, Clim. Dynam., 28, 683–702, https://doi.org/10.1007/s00382-006-0205-x, 2007.

Grimm, A.: Interannual Climate Variability in South America: Impacts on Seasonal Precipitation, Extreme Events, and Possible Effects of Climate Change, Stoch. Env. Res. Risk Assess., 25, 537–554, https://doi.org/10.1007/s00477-010-0420-1, 2011.

Hansen, F., Kruschke, T., Greatbatch, R. J., and Weisheimer, A.: Factors Influencing the Seasonal Predictability of Northern Hemisphere Severe Winter Storms, Geophysical Research Letters, 46, 365–373, https://doi.org/10.1029/2018GL079415, 2019.

Hersbach, H., Bell, B., Berrisford, P., Hirahara, S., Horányi, A., Muñoz-Sabater, J., Nicolas, J., Peubey, C., Radu, R., Schepers, D., Simmons, A., Soci, C., Abdalla, S., Abellan, X., Balsamo, G., Bechtold, P., Biavati, G., Bidlot, J., Bonavita, M., De Chiara, G., Dahlgren, P., Dee, D., Diamantakis, M., Dragani, R., Flemming, J., Forbes, R., Fuentes, M., Geer, A., Haimberger, L., Healy, S., Hogan, R. J., Hólm, E., Janisková, M., Keeley, S., Laloyaux, P., Lopez, P., Lupu, C., Radnoti, G., de Rosnay, P., Rozum, I., Vamborg, F., Villaume, S., and Thépaut, J.-N.: The ERA5 global reanalysis, Q. J. R. Meteorol. Soc., 146, 1999–2049, https://doi.org/10.1002/qj.3803, 2020.

Hillier, J., Matthews, T., Wilby, R., and Murphy, C.: Multi-hazard dependencies can increase or decrease risk, Nat. Clim. Chang., 10, 1–4, https://doi.org/10.1038/s41558-020-0832-y, 2020.

Hillier, J. K., Macdonald, N., Leckebusch, G. C., and Stavrinides, A.: Interactions between apparently 'primary' weather-driven hazards and their cost, Environmental Research Letters, 10, 104 003, https://doi.org/10.1088/1748-9326/10/10/104003, 2015.

Hong Lee, J., Julien, P. Y., and Lee, S.: Teleconnection of ENSO extreme events and precipitation variability over the United States, Journal of Hydrology, 619, 129 206, https://doi.org/10.1016/j.jhydrol.2023.129206, 2023.

Hu, S., Zhang, W., Jin, F.-F., Hong, L.-C., Jiang, F., and Stuecker, M. F.: Seasonal dependence of the Pacific–North American teleconnection associated with ENSO and its interaction with the annual cycle, Journal of Climate, 36, 7061–7072, 2023.

Hurrell, J. W.: Decadal trends in the North Atlantic oscillation: Regional temperatures and precipitation, Science, 269, 676–679, https://doi.org/10.1126/science.269.5224.676, 1995.

Hurrell, J. W. and Deser, C.: North Atlantic climate variability: The role of the North Atlantic Oscillation, Journal of Marine Systems, 79, 231–244, https://doi.org/10.1016/j.jmarsys.2009.11.002, impact of climate variability on marine ecosystems: A comparative approach, 2010.

Hurrell, J. W., Kushnir, Y., Ottersen, G., and Visbeck, M.: An Overview of the North Atlantic Oscillation, pp. 1–35, American Geophysical Union (AGU), ISBN 9781118669037, https://doi.org/10.1029/134GM01, 2003.

IPCC: *Managing the Risks of Extreme Events and Disasters to Advance Climate Change Adaptation. Special Report of Working Groups I and II of the Intergovernmental Panel on Climate Change* [Allen, Simon and Barros, Vicente and (Canada, Ian and (UK, Diarmid and Cardona, Omar and Cutter, Susan and Dube, Opha Pauline and Ebi, Kristie and (USA, Christopher and Handmer, John and (Australia,

Padma and Lavell, Allan and (USA, Katharine and Mastrandrea, Michael and Mcbean, Gordon and Mechler, Reinhard and (UK, Tom and Nicholls, Neville and (Norway, Karen and (USA, Thomas].., https://doi.org/10.13140/2.1.3117.9529, 2012.

665 IPCC: *Climate Change 2021: The Physical Science Basis. Contribution of Working Group I to the Sixth Assessment Report of the Intergovernmental Panel on Climate Change* [Masson-Delmotte, V., P. Zhai, A. Pirani, S.L. Connors, C. Péan, S. Berger, N. Caud, Y. Chen, L. Goldfarb, M.I. Gomis, M. Huang, K. Leitzell, E. Lonnoy, J.B.R. Matthews, T.K. Maycock, T. Waterfield, O. Yelekçi, R. Yu, and B. Zhou (eds.)]., Cambridge University Press. In Press., 2021.

Iturbide, M., Gutiérrez, J. M., Alves, L. M., Bedia, J., Cerezo-Mota, R., Cimadevilla, E., Cofiño, A. S., Di Luca, A., Faria, S. H., Gorodet-
670 skaya, I. V., Hauser, M., Herrera, S., Hennessy, K., Hewitt, H. T., Jones, R. G., Krakovska, S., Manzanas, R., Martínez-Castro, D., Narisma, G. T., Nurhati, I. S., Pinto, I., Seneviratne, S. I., van den Hurk, B., and Vera, C. S.: An update of IPCC climate reference regions for subcontinental analysis of climate model data: definition and aggregated datasets, Earth System Science Data, 12, 2959–2970, https://doi.org/10.5194/essd-12-2959-2020, 2020.

Jeong, D. I., Cannon, A. J., and Morris, R. J.: Projected changes to wind loads coinciding with rainfall for building design in Canada based
675 on an ensemble of Canadian regional climate model simulations, Climatic Change, 162, 821–835, https://doi.org/10.1007/s10584-020-02745-y, 2020.

Jiang, S., Tarasova, L., Yu, G., and Zscheischler, J.: Compounding effects in flood drivers challenge estimates of extreme river floods, Science Advances, 10, eadl4005, https://doi.org/10.1126/sciadv.adl4005, 2024.

Jiménez-Esteve, B. and Domeisen, D.: Nonlinearity in the North Pacific atmospheric response to a linear ENSO forcing, Geophysical Re-
680 search Letters, 46, 2271–2281, 2019.

Jiménez-Esteve, B. and Domeisen, D. I.: Nonlinearity in the tropospheric pathway of ENSO to the North Atlantic, Weather and Climate Dynamics, 1, 225–245, 2020.

Jongman, B., Hochrainer-Stigler, S., Feyen, L., CJH, A., Mechler, R., Bouwer, L., Pflug, G., Rojas, R., and Ward, P.: Increasing Stress on Disaster-Risk Finance due to Large Floods, Nature Climate Change, 4, https://doi.org/10.1038/NCLIMATE2124, 2014.

685 Kawamura, R., Suppiah, R., Collier, M. A., and Gordon, H. B.: Lagged relationships between ENSO and the Asian Summer Monsoon in the CSIRO coupled model, Geophysical Research Letters, 31, https://doi.org/https://doi.org/10.1029/2004GL021411, 2004.

Kay, J. E., Deser, C., Phillips, A., Mai, A., Hannay, C., Strand, G., Arblaster, J. M., Bates, S. C., Danabasoglu, G., Edwards, J., Holland, M., Kushner, P., Lamarque, J.-F., Lawrence, D., Lindsay, K., Middleton, A., Munoz, E., Neale, R., Oleson, K., Polvani, L., and Vertenstein, M.: The Community Earth System Model (CESM) Large Ensemble Project: A Community Resource for Studying Climate Change in the Pres-
690 ence of Internal Climate Variability, Bulletin of the American Meteorological Society, 96, 1333 – 1349, https://doi.org/10.1175/BAMS-D-13-00255.1, 2015.

Kelder, T., Wanders, N., van der Wiel, K., Marjoribanks, T. I., Slater, L. J., l Wilby, R., and Prudhomme, C.: Interpreting extreme climate impacts from large ensemble simulations—are they unseen or unrealistic?, Environmental Research Letters, 17, 044 052, https://doi.org/10.1088/1748-9326/ac5cf4, 2022.

695 Khouakhi, A., Villarini, G., and Vecchi, G.: Contribution of Tropical Cyclones to Rainfall at the Global Scale, Journal of Climate, 30, 359–372, https://doi.org/10.1175/JCLI-D-16-0298.1, 2016.

Kim, W., Iizumi, T., and Nishimori, M.: Global Patterns of Crop Production Losses Associated with Droughts from 1983 to 2009, Journal of Applied Meteorology and Climatology, 58, 1233 – 1244, https://doi.org/10.1175/JAMC-D-18-0174.1, 2019.

King, M., Keenlyside, N., and Li, C.: ENSO teleconnections in terms of non-NAO and NAO atmospheric variability, Clim Dyn, 61,
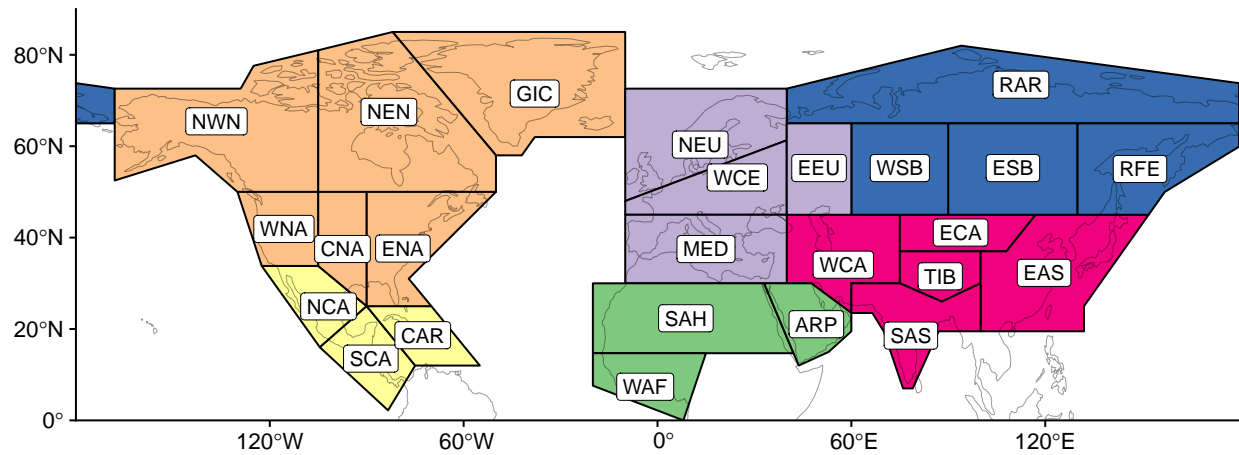700 27172 733, https://doi.org/10.1007/s00382-023-06697-8, 2023.

Kirov, B. and Georgieva, K.: Long-term variations and interrelations of ENSO, NAO and solar activity, Physics and Chemistry of the Earth, Parts A/B/C, 27, 441–448, https://doi.org/https://doi.org/10.1016/S1474-7065(02)00024-4, 2002.

Klawa, M. and Ulbrich, U.: A model for the estimation of storm losses and the identification of severe winter storms in Germany, Natural Hazards and Earth System Science, 3, https://doi.org/10.5194/nhess-3-725-2003, 2003.

705 Knight, J. R., Folland, C. K., and Scaife, A. A.: Climate impacts of the Atlantic Multidecadal Oscillation, Geophysical Research Letters, 33, https://doi.org/https://doi.org/10.1029/2006GL026242, 2006.

Kossin, J. P., Camargo, S. J., and Sitkowski, M.: Climate Modulation of North Atlantic Hurricane Tracks, Journal of Climate, 23, 3057 – 3076, https://doi.org/10.1175/2010JCLI3497.1, 2010.

Kretschmer, M., Adams, S. V., Arribas, A., Prudden, R., Robinson, N., Saggioro, E., and Shepherd, T. G.: Quantifying Causal Pathways
710 of Teleconnections, Bulletin of the American Meteorological Society, 102, E2247 – E2263, https://doi.org/10.1175/BAMS-D-20-0117.1, 2021.

Kurniadi, A., Weller, E., Min, S.-K., and Seong, M.-G.: Independent ENSO and IOD impacts on rainfall extremes over Indonesia, International Journal of Climatology, 41, 3640–3656, https://doi.org/10.1002/joc.7040, 2021.

Lenssen, N. J., Goddard, L., and Mason, S.: Seasonal forecast skill of ENSO teleconnection maps, Weather and Forecasting, 35, 2387–2406,
715 2020.

Li, D., Chen, Y., Messmer, M., Zhu, Y., Feng, J., Yin, B., and Bevacqua, E.: Compound Wind and Precipitation Extremes Across the Indo-Pacific: Climatology, Variability, and Drivers, Geophysical Research Letters, 49, e2022GL098 594, https://doi.org/10.1029/2022GL098594, e2022GL098594 2022GL098594, 2022.

Li, D., Zscheischler, J., Chen, Y., Yin, B., Feng, J., Freund, M., Qi, J., Zhu, Y., and Bevacqua, E.: Intensification and Poleward Shift of
720 Compound Wind and Precipitation Extremes in a Warmer Climate, Geophysical Research Letters, 51, e2024GL110 135, 2024.

Li, W., Zhai, P., and Cai, J.: Research on the Relationship of ENSO and the Frequency of Extreme Precipitation Events in China, Advances in Climate Change Research, 2, 101–107, https://doi.org/10.3724/SP.J.1248.2011.00101, 2011.

Li, Z., Liu, J., Mauzerall, D. L., Li, X., Fan, S., Horowitz, L. W., He, C., Yi, K., and Tao, S.: A potential large and persistent black carbon forcing over Northern Pacific inferred from satellite observations, Scientific Reports, 7, 43 429, https://doi.org/10.1038/srep43429, 2017.

725 Liberato, M. L.: The 19 January 2013 windstorm over the North Atlantic: large-scale dynamics and impacts on Iberia, Weather. Clim. Extremes, 5-6, 16–28, https://doi.org/10.1016/j.wace.2014.06.002, 2014.

Liu, B., Chen, J., Chen, X., Lian, Y., and Wu, L.: Uncertainty in determining extreme precipitation thresholds, Journal of Hydrology, 503, 233–245, https://doi.org/https://doi.org/10.1016/j.jhydrol.2013.09.002, 2013.

Liu, H., Li, D., Chen, Q., Feng, J., Qi, J., and Yin, B.: The multiscale variability of global extreme wind and wave events and their relationships
730 with climate modes, Ocean Engineering, 307, 118 239, https://doi.org/https://doi.org/10.1016/j.oceaneng.2024.118239, 2024.

Lodise, J., Merrifield, S., Collins, C., Rogowski, P., Behrens, J., and Terrill, E.: Global Climatology of Extratropical Cyclones From a New Tracking Approach and Associated Wave Heights From Satellite Radar Altimeter, Journal of Geophysical Research: Oceans, 127, e2022JC018 925, https://doi.org/10.1029/2022JC018925, e2022JC018925 2022JC018925, 2022.

Luca, P. D., Hillier, J. K., Wilby, R. L., Quinn, N. W., and Harrigan, S.: Extreme multi-basin flooding linked with extra-tropical cyclones,
735 Environmental Research Letters, 12, 114 009, https://doi.org/10.1088/1748-9326/aa868e, 2017.

Maher, N., Milinski, S., and Ludwig, R.: Large ensemble climate model simulations: introduction, overview, and future prospects for utilising multiple types of large ensemble, Earth System Dynamics, 12, 401–418, https://doi.org/10.5194/esd-12-401-2021, 2021.

Manning, C., Widmann, M., Bevacqua, E., Loon, A. F. V., Maraun, D., and Vrac, M.: Soil Moisture Drought in Europe: A Compound Event of Precipitation and Potential Evapotranspiration on Multiple Time Scales, J. Hydrometeorol., 19, 1255–1271, https://doi.org/10.1175/JHM-D-18-0017.1, 2018.

Manning, C., Kendon, E. J., Fowler, H. J., Catto, J. L., Chan, S. C., and Sansom, P. G.: Compound wind and rainfall extremes: Drivers and future changes over the UK and Ireland, Weather and Climate Extremes, 44, 100 673, https://doi.org/10.1016/j.wace.2024.100673, 2024.

Maraun, D.: Bias Correcting Climate Change Simulations - A Critical Review, Curr. Clim. Chang. Reports, 2, 211–220, https://doi.org/10.1007/s40641-016-0050-x, 2016.

Martius, O., Pfahl, S., and Chevalier, C.: A global quantification of compound precipitation and wind extremes, Geophys. Res. Lett., 43, 7709–7717, https://doi.org/10.1002/2016GL070017, 2016.

Matthews, T., Murphy, C., Wilby, R. L., and Harrigan, S.: Stormiest winter on record for Ireland and UK, Nature Climate Change, 4, 738–740, https://doi.org/10.1038/nclimate2336, 2014.

Messmer, M. and Simmonds, I.: Global analysis of cyclone-induced compound precipitation and wind extreme events, Weather. Clim. Extremes, 32, 100 324, https://doi.org/10.1016/j.wace.2021.100324, 2021.

Mirrahimi, S., Lim, C. H., and Surat, S.: Review of method to estimation of wind-driven rain on building façade, Advances in Environmental Biology, 9, 18–23, 2015.

Müller, W. A. and Roeckner, E.: ENSO impact on midlatitude circulation patterns in future climate change projections, Geophysical Research Letters, 33, L05711, https://doi.org/10.1029/2005GL025032, 2006.

Nowack, P., Runge, J., Eyring, V., and Haigh, J. D.: Causal networks for climate model evaluation and constrained projections, Nature Communications, 11, 1415, https://doi.org/10.1038/s41467-020-15195-y, 2020.

O'Reilly, C. H., Drouard, M., Ayarzagüena, B., Ambaum, M. H. P., and Methven, J.: The role of storm-track dynamics in the intraseasonal variability of the winter ENSO teleconnection to the North Atlantic, Quarterly Journal of the Royal Meteorological Society, 150, 2069–2086, https://doi.org/10.1002/qj.4691, 2024.

Osman, M., Domeisen, D., Robertson, A. W., and Weisheimer, A.: Sub-seasonal to decadal predictions in support of climate services, Climate Services, 30, 100 397, 2023.

Owen, L. E., Catto, J. L., Stephenson, D. B., and Dunstone, N. J.: Compound precipitation and wind extremes over Europe and their relationship to extratropical cyclones, Weather. Clim. Extremes, 33, 100 342, https://doi.org/10.1016/j.wace.2021.100342, 2021.

Pearl, J.: Linear Models: A Useful "Microscope" for Causal Analysis, Journal of Causal Inference, 1, 155–170, https://doi.org/doi:10.1515/jci-2013-0003, 2013.

Phillips, A., Deser, C., and Fasullo, J.: Evaluating Modes of Variability in Climate Models, Eos, Transactions American Geophysical Union, 95, https://doi.org/10.1002/2014EO490002, 2014.

Pilorz, W., Laskowski, I., Surowiecki, A., and Łupikasza, E.: Fatalities related to sudden meteorological events across Central Europe from 2010 to 2020, International Journal of Disaster Risk Reduction, 88, 103 622, https://doi.org/10.1016/j.ijdrr.2023.103622, 2023.

Pinto, J. G., Zacharias, S., Fink, A. H., Leckebusch, G. C., and Ulbrich, U.: Factors contributing to the development of extreme North Atlantic cyclones and their relationship with the NAO, Climate Dynamics, 32, 711–737, https://doi.org/10.1007/s00382-008-0396-4, 2009.

Priestley, M. D. K., Stephenson, D. B., Scaife, A. A., Bannister, D., Allen, C. J. T., and Wilkie, D.: Return levels of extreme European windstorms, their dependency on the North Atlantic Oscillation, and potential future risks, Natural Hazards and Earth System Sciences, 23, 3845–3861, https://doi.org/10.5194/nhess-23-3845-2023, 2023.

775   Qian, C., Ye, Y., Bevacqua, E., and Zscheischler, J.: Human influences on spatially compounding flooding and heatwave events in China and future increasing risks, Weather and Climate Extremes, 42, 100 616, https://doi.org/10.1016/j.wace.2023.100616, 2023.

Qiu, Y., Cai, W., Guo, X., and Ng, B.: The asymmetric influence of the positive and negative IOD events on China's rainfall, Scientific Reports, 4, 4943, https://doi.org/10.1038/srep04943, 2014.

Raible, C. C.: On the relation between extremes of midlatitude cyclones and the atmospheric circulation using ERA40, Geophysical Research
780   Letters, 34, https://doi.org/https://doi.org/10.1029/2006GL029084, 2007.

Ralph, F. M., Neiman, P. J., Wick, G. A., Gutman, S. I., Dettinger, M. D., Cayan, D. R., and White, A. B.: Flooding on California's Russian River: Role of atmospheric rivers, Geophysical Research Letters, 33, https://doi.org/https://doi.org/10.1029/2006GL026689, 2006.

Rappaport, E.: Loss of Life in the United States Associated with Recent Atlantic Tropical Cyclones, Bulletin of The American Meteorological Society - BULL AMER METEOROL SOC, 81, https://doi.org/10.1175/1520-0477(2000)081<2065:LOLITU>2.3.CO;2, 2000.

785   Rasmijn, L., Schrier, G., Bintanja, R., Barkmeijer, J., Sterl, A., and Hazeleger, W.: Future equivalent of 2010 Russian heatwave intensified by weakening soil moisture constraints, Nature Climate Change, 8, 1–5, https://doi.org/10.1038/s41558-018-0114-0, 2018.

Raveh-Rubin, S. and Catto, J. L.: Climatology and dynamics of the link between dry intrusions and cold fronts during winter, Part II: Front-centred perspective, Climate Dynamics, 53, 1893–1909, https://doi.org/10.1007/s00382-019-04793-2, 2019.

Raveh-Rubin, S. and Wernli, H.: Large-scale wind and precipitation extremes in the Mediterranean: a climatological analysis for 1979–2012,
790   Q. J. Roy. Meteor. Soc., 141, 2404–2417, https://doi.org/10.1002/qj.2531, 2015.

Raymond, C., Suarez-Gutierrez, L., Kornhuber, K., Pascolini-Campbell, M., Sillmann, J., and Waliser, D. E.: Increasing spatiotemporal proximity of heat and precipitation extremes in a warming world quantified by a large model ensemble, Environ. Res. Lett., 17, 035 005, https://doi.org/10.1088/1748-9326/ac5712, 2022.

Renwick, J. A. and Wallace, J. M.: Relationships between North Pacific Wintertime Blocking, El Niño, and the PNA Pattern, Monthly
795   Weather Review, 124, 2071 – 2076, https://doi.org/10.1175/1520-0493(1996)124<2071:RBNPWB>2.0.CO;2, 1996.

Ridder, N., Ukkola, A., Pitman, A., and Perkins-Kirkpatrick, S.: Increased occurrence of high impact compound events under climate change, NPJ Clim. Atmos. Sci., 5, https://doi.org/10.1038/s41612-021-00224-4, 2022.

Roberts, J. F., Champion, A. J., Dawkins, L. C., Hodges, K. I., Shaffrey, L. C., Stephenson, D. B., Stringer, M. A., Thornton, H. E., and Youngman, B. D.: The XWS open access catalogue of extreme European windstorms from 1979 to 2012, Nat. Hazards Earth Syst. Sci.,
800   14, 2487–2501, https://doi.org/10.5194/nhess-14-2487-2014, 2014.

Ruiz-Barradas, A., Carton, J. A., and Nigam, S.: Structure of Interannual-to-Decadal Climate Variability in the Tropical Atlantic Sector, Journal of Climate, 13, 3285 – 3297, https://doi.org/10.1175/1520-0442(2000)013<3285:SOITDC>2.0.CO;2, 2000.

Schär, C., Ban, N., Fischer, E. M., Rajczak, J., Schmidli, J., Frei, C., Giorgi, F., Karl, T. R., Kendon, E. J., Tank, A. M. G. K., O'Gorman, P. A., Sillmann, J., Zhang, X., and Zwiers, F. W.: Percentile indices for assessing changes in heavy precipitation events, Climatic Change,
805   137, 201–216, https://doi.org/10.1007/s10584-016-1669-2, 2016.

Schmidt, N., Lipp, E. K., Rose, J. B., and Luther, M. E.: ENSO Influences on Seasonal Rainfall and River Discharge in Florida, Journal of Climate, 14, 615 – 628, https://doi.org/10.1175/1520-0442(2001)014<0615:EIOSRA>2.0.CO;2, 2001.

Sedgwick, P.: Multiple hypothesis testing and Bonferroni's correction, BMJ, 349, https://doi.org/10.1136/bmj.g6284, 2014.

Seneviratne, S., Nicholls, N., Easterling, D., Goodess, C., Kanae, S., Kossin, J., Luo, Y., Marengo, J., McInnes, K., Rahimi, M., Reichstein,
810   M., Sorteberg, A., Vera, C., and Zhang, X.: Changes in climate extremes and their impacts on the natural physical environment. In: *Managing the Risks of Extreme Events and Disasters to Advance Climate Change Adaptation* [Field, C.B., V. Barros, T.F. Stocker, D.

Qin, D.J. Dokken, K.L. Ebi, M.D. Mastrandrea, K.J. Mach, G.-K. Plattner, S.K. Allen, M. Tignor, and P.M. Midgley (eds.)], pp. 109–230, 2012.

Singh, J., Ashfaq, M., Skinner, C. B., Anderson, W. B., and Singh, D.: Amplified risk of spatially compounding droughts during co-occurrences of modes of natural ocean variability, npj Climate and Atmospheric Science, 4, 7, https://doi.org/10.1038/s41612-021-00161-2, 2021.

Stuecker, M. F., Timmermann, A., Jin, F.-F., Chikamoto, Y., Zhang, W., Wittenberg, A. T., Widiasih, E., and Zhao, S.: Revisiting ENSO/Indian Ocean dipole phase relationships, Geophysical Research Letters, 44, 2481–2492, 2017.

Toniazzo, T. and Scaife, A. A.: The influence of ENSO on winter North Atlantic climate, Geophysical Research Letters, 33, https://doi.org/https://doi.org/10.1029/2006GL027881, 2006.

Trascasa-Castro, P., Ruprich-Robert, Y., Castruccio, F., and Maycock, A. C.: Warm Phase of AMV Damps ENSO Through Weakened Thermocline Feedback, Geophysical Research Letters, 48, e2021GL096 149, https://doi.org/10.1029/2021GL096149, e2021GL096149 2021GL096149, 2021.

van den Hurk, B. J., White, C. J., Ramos, A. M., Ward, P. J., Martius, O., Olbert, I., Roscoe, K., Goulart, H. M., and Zscheischler, J.: Consideration of compound drivers and impacts in the disaster risk reduction cycle, iScience, 26, 106 030, https://doi.org/10.1016/j.isci.2023.106030, 2023.

van der Wiel, K., Bloomfield, H. C., Lee, R. W., Stoop, L. P., Blackport, R., Screen, J. A., and Selten, F. M.: The influence of weather regimes on European renewable energy production and demand, Environmental Research Letters, 14, 094 010, https://doi.org/10.1088/1748-9326/ab38d3, 2019.

van Oldenborgh, G. J., Philip, S. Y., and Collins, M.: El Niño in a changing climate: a multi-model study, Ocean Science, 1, 81–95, https://doi.org/10.5194/os-1-81-2005, 2005.

Van Stan, J., Siegert, C., Levia, D., and Scheick, C.: Effects of wind-driven rainfall on stemflow generation between codominant tree species with differing crown characteristics, Agricultural and Forest Meteorology, 151, 1277, https://doi.org/10.1016/j.agrformet.2011.05.008, 2011.

Vignotto, E., Engelke, S., and Zscheischler, J.: Clustering bivariate dependencies of compound precipitation and wind extremes over Great Britain and Ireland, Weather and Climate Extremes, 32, 100 318, https://doi.org/https://doi.org/10.1016/j.wace.2021.100318, 2021.

Wahl, T., Jain, S., Bender, J., Meyers, S., and Luther, M.: Increasing risk of compound flooding from storm surge and rainfall for major US cities, Nat. Clim. Chang., 5, 1093–1097, https://doi.org/10.1038/nclimate2736, 2015.

Waliser, D. and Guan, B.: Extreme winds and precipitation during landfall of atmospheric rivers, Nature Geoscience, 10, 179–183, https://doi.org/10.1038/ngeo2894, 2017.

Wallace, J. M. and Gutzler, D. S.: Teleconnections in the Geopotential Height Field during the Northern Hemisphere Winter, Monthly Weather Review, 109, 784 – 812, https://doi.org/10.1175/1520-0493(1981)109<0784:TITGHF>2.0.CO;2, 1981.

Wang, C.: Three-ocean interactions and climate variability: a review and perspective, Climate Dynamics, 53, 5119–5136, https://doi.org/10.1007/s00382-019-04930-x, 2019.

Wang, J., Chen, Y., Tett, S. F. B., Stone, D., Nie, J., Feng, J., Yan, Z., Zhai, P., and Ge, Q.: Storyline attribution of human influence on a record-breaking spatially compounding flood-heat event, Science Advances, 9, eadi2714, https://doi.org/10.1126/sciadv.adi2714, 2023.

Whan, K. and Zwiers, F.: The impact of ENSO and the NAO on extreme winter precipitation in North America in observations and regional climate models, Climate Dynamics, 48, 1401–1411, https://doi.org/10.1007/s00382-016-3148-x, 2017.

White, C. J., Domeisen, D. I., Acharya, N., Adefisan, E. A., Anderson, M. L., Aura, S., Balogun, A. A., Bertram, D., Bluhm, S., Brayshaw, D. J., et al.: Advances in the application and utility of subseasonal-to-seasonal predictions, Bulletin of the American Meteorological Society, 103, E1448–E1472, 2022.

Williams, G. P.: Bank-full discharge of rivers, Water Resources Research, 14, 1141–1154, https://doi.org/https://doi.org/10.1029/WR014i006p01141, 1978.

Xie, N., Sun, Y., and Gao, M.: The Influence of Five Teleconnection Patterns on Wintertime Extratropical Cyclones over Northwest Pacific, Atmosphere, 11, https://doi.org/10.3390/atmos11111248, 2020.

Xing, Z., Yu, Z., Wei, J., Zhang, X., Ma, M., Yi, P., Ju, Q., Wang, J., Laux, P., and Kunstmann, H.: Lagged influence of ENSO regimes on droughts over the Poyang Lake basin, China, Atmospheric Research, 275, 106 218, https://doi.org/10.1016/j.atmosres.2022.106218, 2022.

Xue, J., Luo, J.-J., Zhang, W., and Yamagata, T.: ENSO–IOD Inter-Basin Connection Is Controlled by the Atlantic Multidecadal Oscillation, Geophysical Research Letters, 49, e2022GL101 571, 2022.

Yeh, S.-W., Cai, W., Min, S.-K., McPhaden, M. J., Dommenget, D., Dewitte, B., Collins, M., Ashok, K., An, S.-I., Yim, B.-Y., and Kug, J.-S.: ENSO Atmospheric Teleconnections and Their Response to Greenhouse Gas Forcing, Reviews of Geophysics, 56, 185–206, https://doi.org/10.1002/2017RG000568, 2018.

Yin, J., Gao, Y., Chen, R., Yu, D., Wilby, R., Wright, N., Ge, Y., Bricker, J., Gong, H., and Guan, M.: Flash floods: why are more of them devastating the world's driest regions?, Nature, 615, 212–215, 2023.

Zhang, X., Alexander, L., Hegerl, G. C., Jones, P., Tank, A. K., Peterson, T. C., Trewin, B., and Zwiers, F. W.: Indices for monitoring changes in extremes based on daily temperature and precipitation data, WIREs Climate Change, 2, 851–870, https://doi.org/https://doi.org/10.1002/wcc.147, 2011.

Zhang, Y., Sun, X., and Chen, C.: Characteristics of concurrent precipitation and wind speed extremes in China, Weather and Climate Extremes, 32, 100 322, https://doi.org/10.1016/j.wace.2021.100322, 2021.

Zhao, H.: On the distinct interannual variability of tropical cyclone activity over the eastern North Pacific, Atmósfera, 28, 161–178, https://www.elsevier.es/en-revista-atmosfera-76-articulo-on-distinct-interannual-variability-tropical-S0187623617300024, 10.20937/ATM.2015.28.03.02, 2015.

Zscheischler, J. and Lehner, F.: Attributing compound events to anthropogenic climate change, Bull. Amer. Meteor. Soc., pp. 1–45, https://doi.org/10.1175/BAMS-D-21-0116.1, 2021.

Zscheischler, J. and Seneviratne, S.: Dependence of drivers affects risks associated with compound events, Sci. Adv, 3, e1700 263, https://doi.org/10.1126/sciadv.1700263, 2017.

Zscheischler, J., Westra, S., Hurk, B., Seneviratne, S., Ward, P., Pitman, A., AghaKouchak, A., Bresch, D., Leonard, M., Wahl, T., and Zhang, X.: Future climate risk from compound events, Nat. Clim. Chang., pp. 469–477, https://doi.org/10.1038/s41558-018-0156-3, 2018.

Zscheischler, J., Martius, O., Westra, S., Bevacqua, E., Raymond, C., Horton, R., Hurk, B., AghaKouchak, A., Jézéquel, A., Mahecha, M., Maraun, D., Ramos, A., Ridder, N., Thiery, W., and Vignotto, E.: A typology of compound weather and climate events, Nat. Rev. Earth Environ., 1, 1–5, 2020.

Figure 1. Presentation of the regions under study, that is the SREX regions (Iturbide et al., 2020) adopted by the Intergovernmental Panel on Climate Change (IPCC) in the Northern Hemisphere. The bottom part shows short and full names of the regions. Regions are clustered in macroareas (see legend). To balance the number of regions between continents, we partitioned the Asian continent into two macroareas (North Asia and Central-South Asia) and included the Arabic Peninsula (ARP) region in the Africa macroarea.
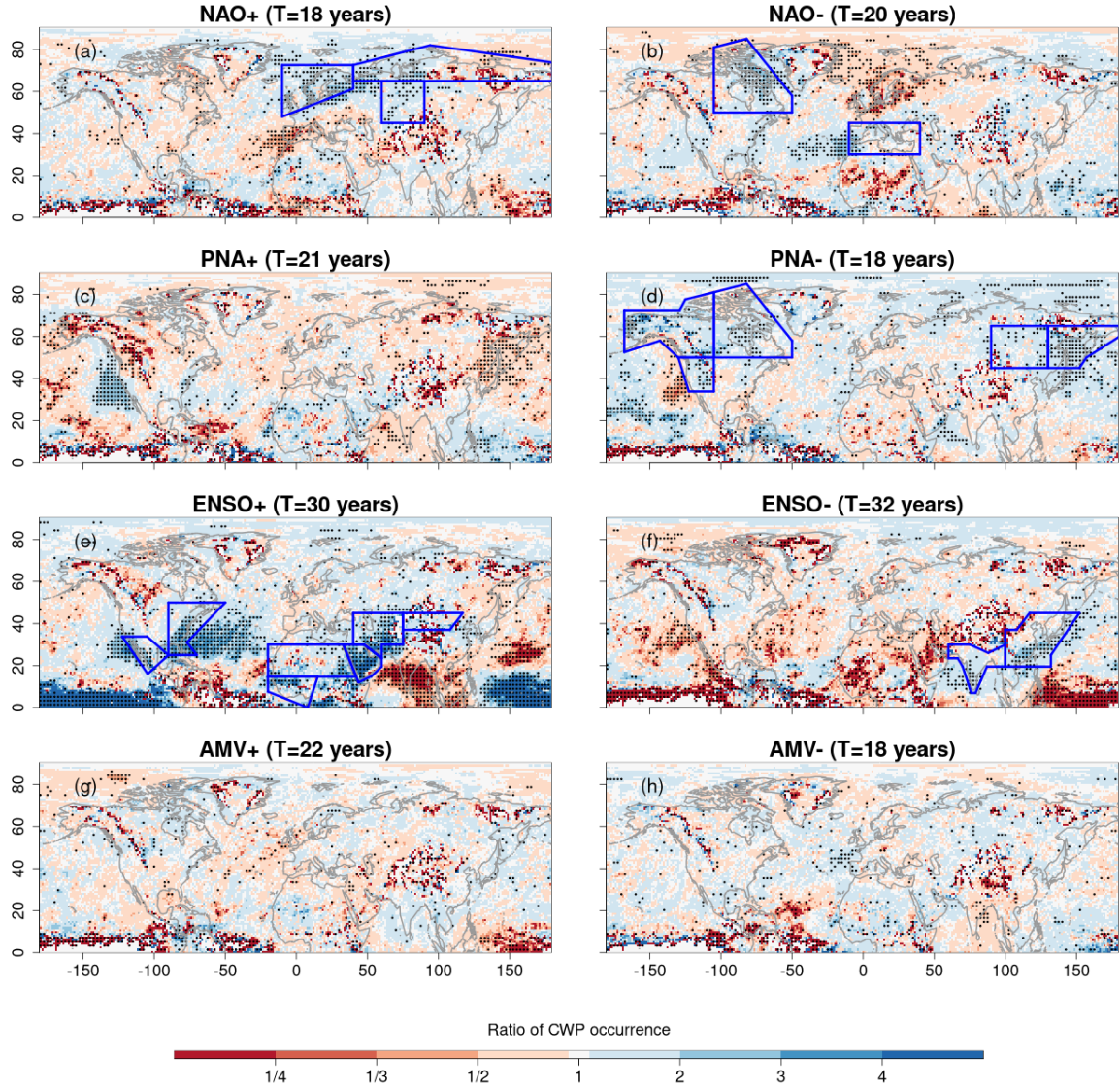
Figure 2. Direct effect of variability modes on wintertime compound wind and precipitation (CWP) extremes. Ratio of the average wintertime (December-February) CWP extreme frequencies for the (a) positive and (b) negative phases of NAO (while other variability modes are in their neutral phases) compared to neutral conditions (all variability modes being in their neutral phases) based on the CESM model. Corresponding maps are also displayed for (c, d) PNA, (e, f) ENSO and (g, h) AMV. Numbers in the headers indicate the conditional empirical return period T (in years) for positive and negative phases of the variability modes (while other modes are in their neutral phases). The empirical return period for neutral conditions (i.e., when all modes are in their neutral phases) is T=3 years. Stippling indicates significant differences of mean frequency relative to neutral conditions at the 10% significance level using permutation tests (two-sided) with Bonferroni correction. The framed regions in blue are those where the direct effects of variability modes significantly increase regionally averaged CWP extreme frequencies compared with neutral conditions (following the methodology defined in subsection 2.2.3, and reflecting information in Fig. 3).
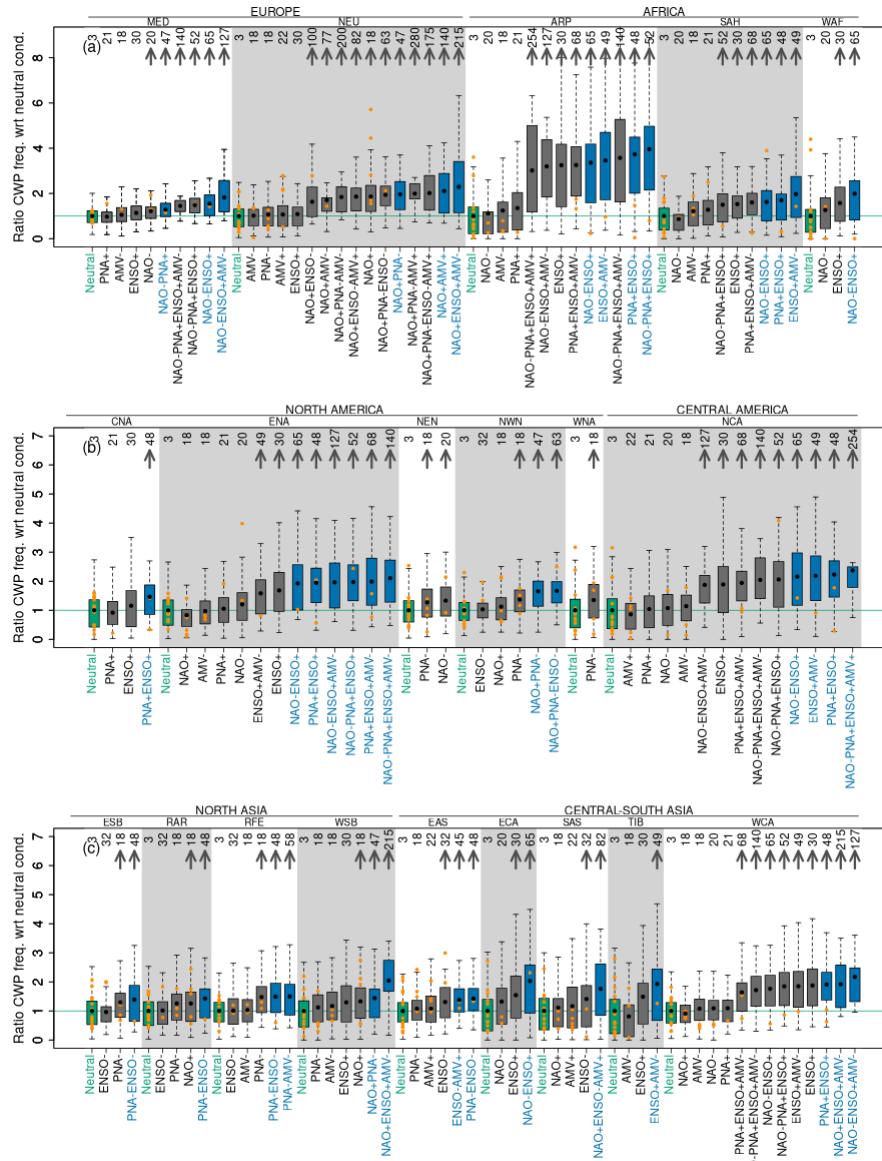
Figure 3. Influence of concurrent variability modes on regional compound wind and precipitation (CWP) extremes. Ratio of the re-gionally averaged wintertime CWP extreme frequencies for the relevant individual and concurrent variability modes (following the method-ology defined in subsection 2.2.3) with respect to average frequency for neutral conditions based on the CESM model (orange dots represent associated values of the ratio derived from ERA5, when available, with each dot representing one winter season). Results are displayed for (a) Europe and Africa, (b) North America and Central America, and (c) Northern Asia and Central-South Asia. The conditional empirical return periods (in years; see Methods) for individual and concurrent variability modes are indicated on the top. Grey arrows indicate sig-nificant differences in the mean frequency relative to neutral conditions (at the 10% significance level, with Bonferroni correction). Green boxes indicate distributions for neutral conditions (all variability modes being in their neutral phases) and green horizontal lines indicate ratios equal to one. Blue boxes indicate mode combinations with amplified effects, that is higher means of regionally averaged CWP extreme frequencies than their underlying mode sub-combinations (methods subsection 2.2.3). We remove concurrent variability modes that occur in less than 10 winters and regions without significant effects arrows (EEU, WCE, GIC, CAR and SCA).
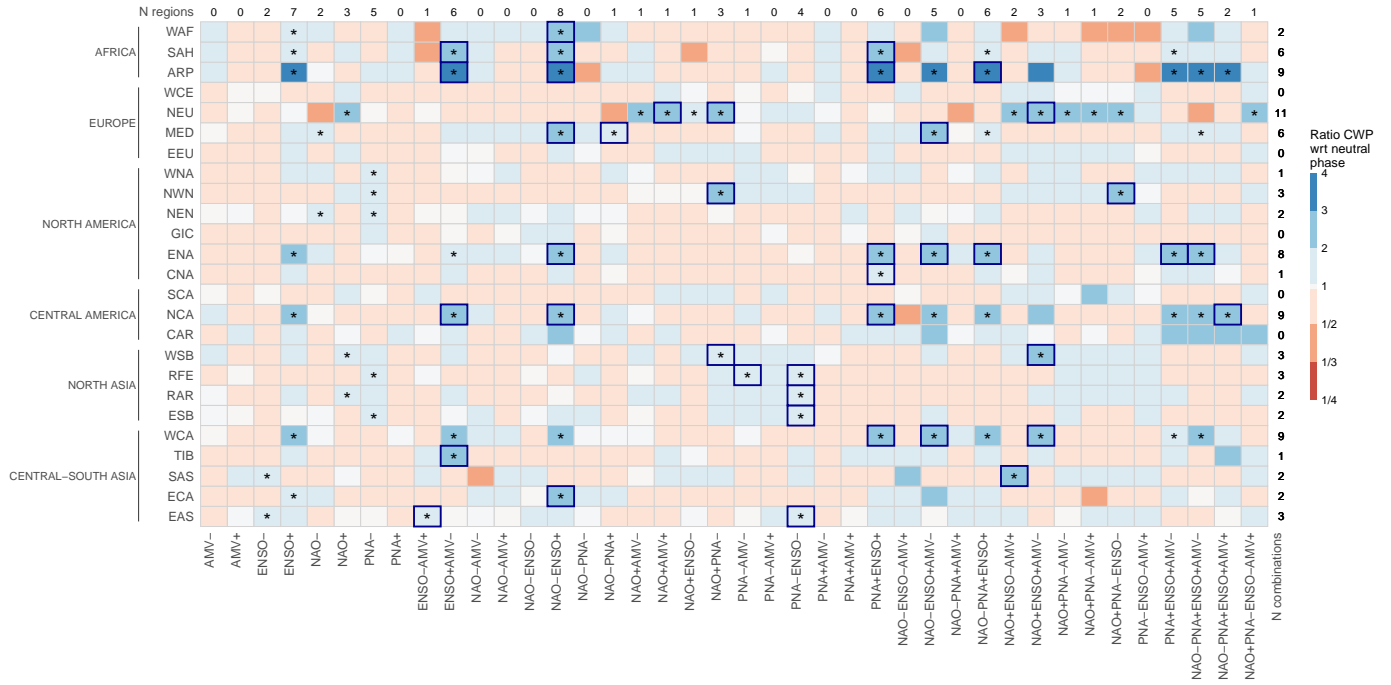
Figure 4. Effects of variability modes on wintertime compound wind and precipitation (CWP) extremes in SREX regions. For different regions (see labels on the left side of the matrix), the ratio of the regionally averaged CWP extreme frequencies for individual and concurrent variability modes (see labels on the bottom side of the matrix) with respect to the average frequency under neutral phases of all modes (Metric 1, see Methods), based on the CESM model. Note that positive effects of concurrent variability modes (ratio above 1) tend to be stronger than negative effects (ratio below 1). The individual and concurrent variability modes with significant effects (at the 10% level with Bonferroni correction) relative to neutral conditions are indicated with an asterisk. Blue cell borders indicate combinations with higher means of regionally averaged CWP extreme frequencies than their underlying mode sub-combinations (methods in subsection 2.2.3). To ensure robustness, we do not display concurrent variability modes that occur in less than 10 winters. Based on the displayed information, the numbers on the top and right margins indicate the total count of regions and mode combinations with significant effects of modes, respectively.
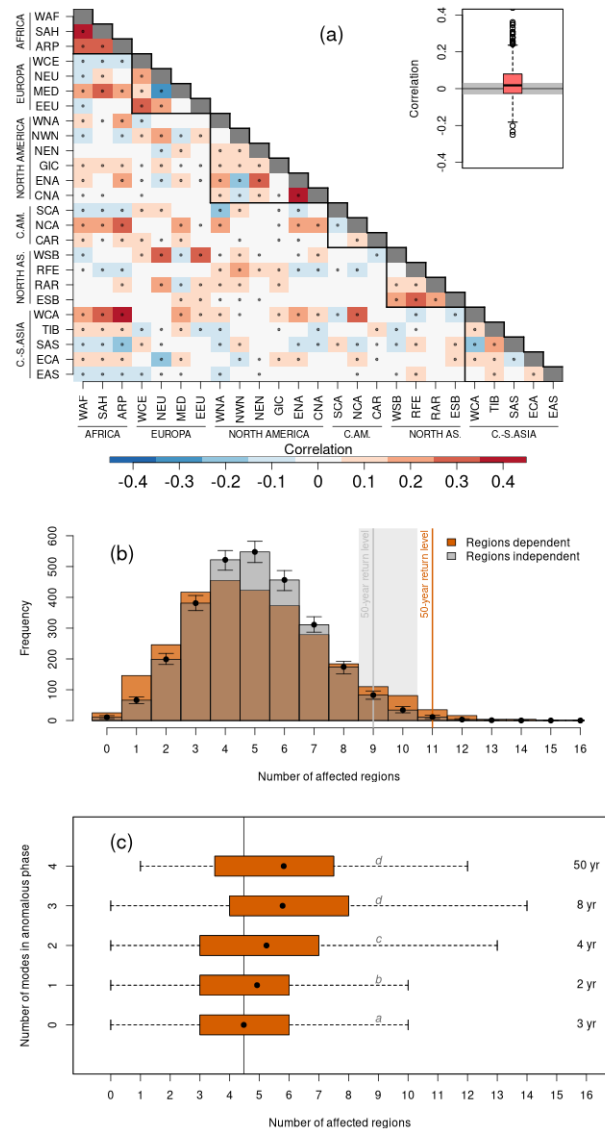
Figure 5. Dependencies between regional wintertime compound wind and precipitation (CWP) extremes. (a) Matrix of Spearman correlations for regionally averaged wintertime (December-February) CWP extreme frequencies between regions based on the CESM model. Stippling indicates significant correlations (correlation values that are outside the 90% centred confidence interval). A contour is added for regions in the same macroarea. The boxplot shows summaries of the distribution of the correlations shown in the matrix (interquartile range, median and outliers); the grey background shows the confidence interval for no correlation (bootstrap-based 90% range). (b) Histograms of the number of regions with a high frequency of CWP extremes during the same winter based on the CESM model (orange histogram) and when assuming independence between regional wintertime CWP extreme frequencies (grey histogram; obtained via shuffling the data 1000 times via bootstrap). Vertical lines show the 50-year return levels under dependence and independence. Bootstrap-based confidence intervals for each bin and 50-year return level at 10% significance level are also shown. (c) Boxplots of the number of affected regions given different numbers of variability modes in anomalous phases. The conditional empirical return periods (in years; see Methods) for the different number of variability modes in anomalous phases are indicated on the right. Mean of the ratios under a different number of modes in anomalous phases that are not significantly different ($\alpha = 0.10$, one-sided permutation test) are indicated with the same letters (Jiang et al., 2024). The average number of regions affected under neutral conditions is indicated by a vertical line.
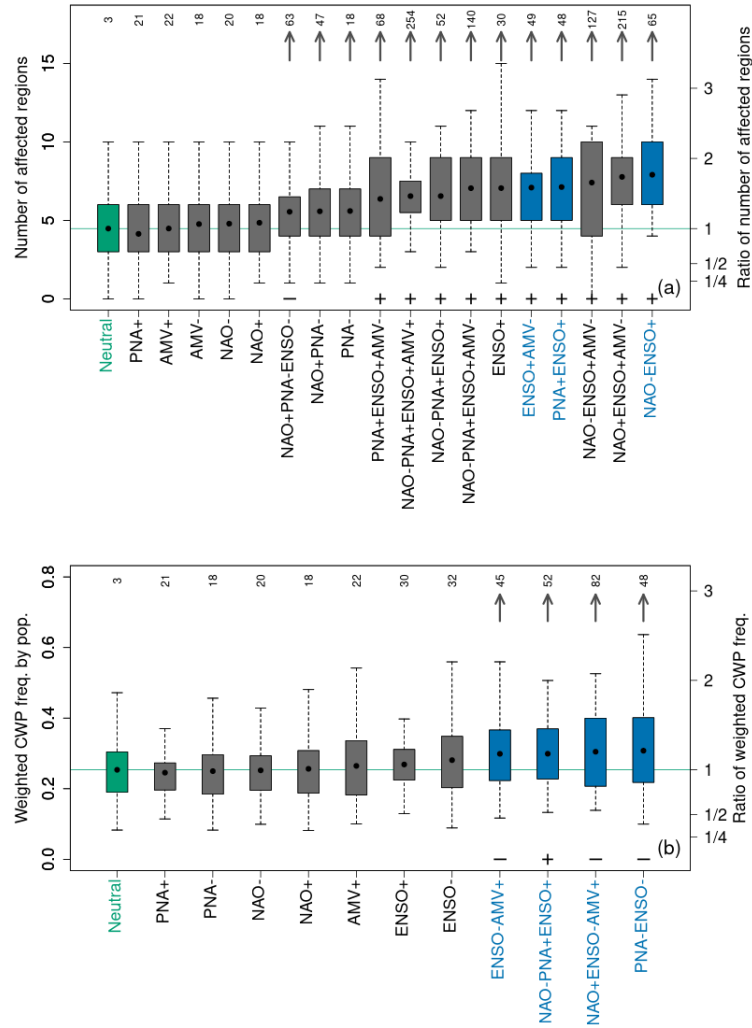
Figure 6. Influence of variability modes on spatially compounding wind and precipitation (CWP) extremes. (a) Distributions of the number of regions (left y-axis) experiencing a high frequency of CWP extremes during the same winter (December-February) for different individual and concurrent variability modes (x-axis), based on the CESM model. The right y-axis shows the ratio of the metric to its average under neutral phases of all modes. The combinations presented are selected according to the methodology defined in subsection 2.2.3. Grey arrows indicate significant differences in the mean with respect to neutral conditions at the 10% significance level using one-sided permutation tests and Bonferroni correction. Green boxes indicate distributions for neutral conditions (all variability modes being in their neutral phases). Blue boxes indicate combinations exhibiting higher means than their underlying mode sub-combinations (methods subsection 2.2.3). (b) The same as panel (a), but for the population-weighted CWP extremes over the Northern Hemisphere. Symbols + and − above the x-axis in panels (a) and (b) highlight combinations having a significant effect for a metric containing ENSO+ and ENSO-, respectively.
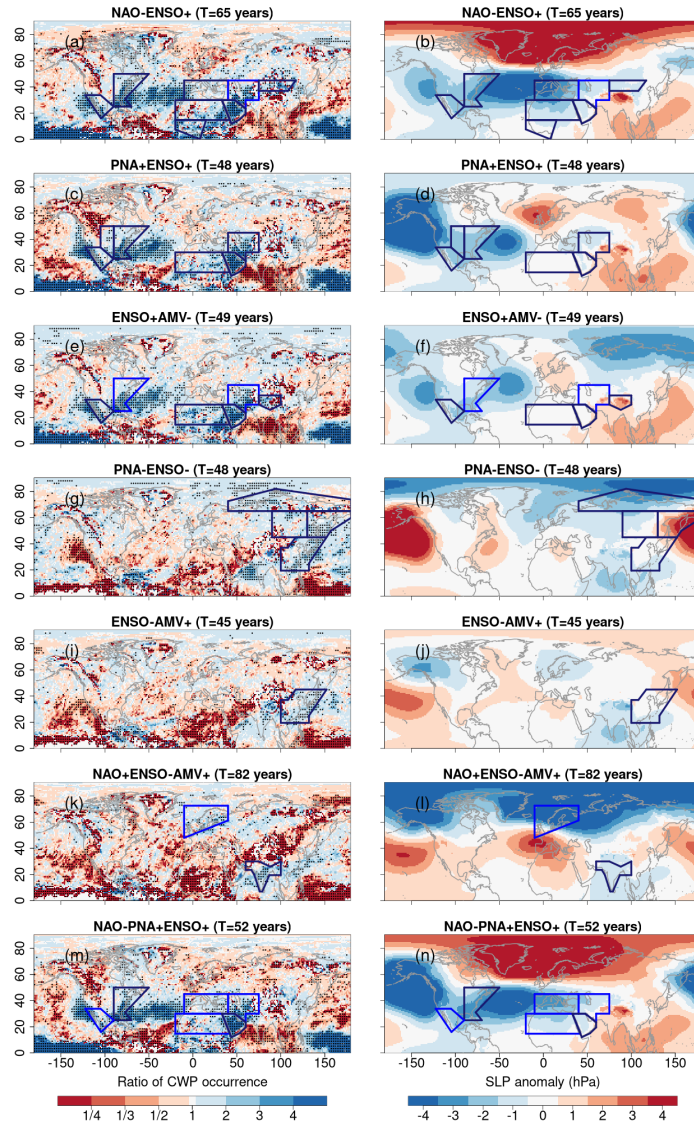
Figure 7. Compound wind and precipitation (CWP) extremes for concurrent anomalies in variability modes and associated sea level pressure anomalies. (a) Ratio of the average wintertime (December-February) CWP frequencies for the concurrent variability mode NAO-ENSO+ (while other variability modes are in their neutral phases) compared to winter with all variability modes in neutral phases, based on the CESM model. (b) Mean sea level pressure anomalies for NAO-ENSO+ (while other variability modes are in their neutral phases) compared to neutral conditions (all variability modes being in their neutral phases) based on the CESM model. Corresponding maps are also displayed for (c, d) PNA+ENSO+, (e, f) ENSO+AMV-, (g, h) PNA-ENSO-, (i, j) ENSO-AMV+, (k, l) NAO+ENSO-AMV+ and (m, n) NAO-PNA+ENSO+. Numbers in the headers indicate the conditional empirical return period T (in years; see Methods) for the different concurrent variability modes stated in the title of the panels, whereas the return period for neutral conditions (all modes are in their neutral phases) is T=3 years. Stippling indicates significant differences in mean frequency relative to neutral conditions at the 10% significance level using permutation tests (two-sided) with Bonferroni correction. The framed regions are those where concurrent variability modes significantly increase regionally averaged CWP extreme frequencies compared with neutral conditions; by reflecting information in Fig. 3, the dark framing indicates an amplified effect with respect to underlying mode sub-combinations (methods in subsection 2.2.3).